Candidate LBV stars in galaxy NGC 7793 found via HST photometry + MUSE spectroscopy

Aida Wofford,[1]* Vanesa Ramírez,[2] Janice C. Lee,[3] David A. Thilker,[4] Lorenza Della Bruna,[5] Angela Adamo,[5] Schuyler D. Van Dyk,[3] Artemio Herrero,[6,7] Hwihyun Kim,[8] Alessandra Aloisi,[9] Daniela Calzetti,[10] Rupali Chandar,[11] Daniel A. Dale,[12] Selma E. de Mink,[13,14] John S. Gallagher,[15] Dimitrios A. Gouliermis,[16,17] Kathryn Grasha,[18,19] Eva K. Grebel,[20] E. Sacchi,[9,21] Linda J. Smith,[9,22] Leonardo Úbeda,[9] Rene A. M. Walterbos,[23] Stephen Hannon,[3,24] Matteo Messa[10]

[1] *Instituto de Astronomía, Universidad Nacional Autónoma de México, Unidad Académica en Ensenada, Km 103 Carr. Tijuana–Ensenada, Ensenada 22860, México*
[2] *Instituto de Física - FCEN, Universidad de Antioquia Calle 70 No. 52-21, Medellín, Colombia*
[3] *Caltech/IPAC, Pasadena, CA 91125*
[4] *Dept. of Physics and Astronomy, The Johns Hopkins University, Baltimore, MD*
[5] *Dept. of Astronomy, The Oskar Klein Centre, Stockholm University, Stockholm, Sweden*
[6] *Instituto de Astrofísica de Canarias, La Laguna, Tenerife, Spain*
[7] *Departamento de Astrofísica, Universidad de La Laguna, Tenerife, Spain*
[8] *Gemini Observatory, Casilla 603, La Serena, Chile*
[9] *Space Telescope Science Institute, 3700 San Martin Drive, Baltimore, MD, USA*
[10] *Dept. of Astronomy, University of Massachusetts – Amherst, Amherst, MA 01003, USA*
[11] *Dept. of Physics and Astronomy, University of Toledo, Toledo, OH, USA*
[12] *Dept. of Physics and Astronomy, University of Wyoming, Laramie, WY, USA*
[13] *Anton Pannenkoek Institute for Astronomy, University of Amsterdam, NL-1090 GE Amsterdam, the Netherlands* [3]*GRAPPA, University of* [14] *Amsterdam, Science Park 904, 1098 XH Amsterdam, The Netherlands* [15] *Dept. of Astronomy, University of Wisconsin–Madison, Madison, WI, USA*
[16] *Zentrum für Astronomie der Universität Heidelberg, Institut für Theoretische Astrophysik, Albert-Ueberle-Str. 2, 69120 Heidelberg, Germany*
[17] *Max Planck Institute for Astronomy, Â̆ Königstuhl 17, 69117 Heidelberg, Germany*
[18] *Research School of Astronomy and Astrophysics, Australian National University, Canberra, ACT 2611, Australia*
[19] *ARC Centre of Excellence for All Sky Astrophysics in 3 Dimensions (ASTRO 3D), Australia*
[20] *Astronomisches Rechen-Institut, Zentrum für Astronomie der Universität Heidelberg, Mönchhofstr. 12–14, 69120 Heidelberg, Germany*
[21] *INAF – OAS Osservatorio di Astrofisica e Scienza dello Spazio, Bologna, Italy*
[22] *European Space Agency*
[23] *Dept. of Astronomy, New Mexico State University, Las Cruces, NM, USA*
[24] *Dept. of Physics & Astronomy, University of California, CA, USA*

ABSTRACT

Only about 19 Galactic and 25 extra-galactic bona-fide Luminous Blue Variables (LBVs) are known to date. This incomplete census prevents our understanding of this crucial phase of massive star evolution which leads to the formation of heavy binary black holes via the classical channel. With large samples of LBVs one could better determine the duration and maximum stellar luminosity which characterize this phase. We search for candidate LBVs (cLBVs) in a new galaxy, NGC 7793. For this purpose, we combine high spatial resolution images from two *Hubble Space Telescope (HST)* programs with optical spectroscopy from the Multi Unit Spectroscopic Explorer (MUSE). By combining PSF-fitting photometry measured on F547M, F657N, and F814W images, with restrictions on point-like appearance (at HST resolution) and Hα luminosity, we find 100 potential cLBVs, 36 of which fall in the MUSE fields. Five of the latter 36 sources are promising cLBVs which have $M_V \leq -7$ and a combination of: Hα with a P-Cygni profile; no [O I] $\lambda6300$ emission; weak or no [O III] $\lambda5007$ emission; large [N II]/Hα relative to H II regions; and [S II] $\lambda6716$/[S II] $\lambda6731 \sim 1$. It is not clear if these five cLBVs are isolated from O-type stars, which would favor the binary formation scenario of LBVs. Our study, which approximately covers one fourth of the optical disc of NGC 7793, demonstrates how by combining the above *HST* surveys with multi-object spectroscopy from 8-m class telescopes, one can efficiently find large samples of cLBVs in nearby galaxies.

Key words: galaxies: individual: NGC 7793 – stars: massive – variables: S Doradus – catalogues

1 INTRODUCTION

Luminous Blue Variables (LBVs), also known as S Doradus variables[1], constitute a rare and poorly-understood phase in the lives of massive stars. This phase is characterized by episodic mass eruptions, very high luminosities[2], the highest mass loss rates among all observed stars[3], and significant photometric and spectroscopic variability. In the Hertzsprung-Russell (H-R) diagram, LBVs are located between the Main Sequence (MS) and the Humphreys-Davidson (H-D) luminosity limit above which only highly unstable objects are found. The lack of Red Supergiant stars of similar luminosity indicates that LBVs cannot evolve to the red, and if they try to, they probably become unstable. Only a limited population of LBVs in outburst phase have been found to the right of the H-D limit.

In the Milky Way and the Magellanic Clouds, LBVs are thought to be responsible for some extra-galactic non-SN transients (Van Dyk & Matheson 2012; Humphreys et al. 2017b). Furthermore, the episodic mass loss of LBVs has been a reference point for interpreting the dense circumstellar material around Type IIn supernovae (SNe, Smith 2017).

Open questions about LBVs concern the total amount of mass lost in a typical eruption and how it scales with initial mass and metallicity, the duty cycle and number of repeated LBV giant eruptions, and whether all stars or only a special subset suffer the LBV giant eruptions (Herrero et al. 2010; Smith 2017).

In the classical "Conti scenario" (Conti 1975), which assumes single-star evolution, LBVs are a short phase (10^4 – 10^5 yr, Herrero et al. 2010) in the lives of the most massive stars ($M_{ZAMS} \geq 40\,M_\odot$), which occurs immediately after H-core exhaustion during the transition to He-core burning. In this scenario, it is the mass loss which occurs during the LBV phase which removes the H envelope of the star, transforming the star into an H-deficient Wolf-Rayet star. In this scenario, stars evolve on times scales of $\leq 3 - 4$ Myr[4] and consequently do not have time to move far from their birthplaces. Thus, one would expect to find LBVs near young O-type MS stars, which observationally, are stars that appear to be clustered (Smith 2019). However, LMC observations show that LBVs are more spatially dispersed than O-type MS stars, which has led Smith & Tombleson (2015) and Smith (2019) to argue that LBVs are likely the products of close binary evolution. This is because the larger spatial dispersion of LBVs can be explained by either SN kicks which move the LBVs far from their birthplace, or rejuvenation via mass transfer and mergers, which produce older massive stars at a time when the single O-type stars have disappeared. In the binary scenario, LBVs would be massive evolved blue stragglers, which in the H-R diagrams of star clusters are MS stars which are more luminous and bluer than stars at the MS turnoff point of the cluster. Note that Davidson et al. (2016) dispute the results of Smith & Tombleson (2015) and argue for the standard view of LBVs.

Not understanding LBV mass loss imprints large uncertainties in massive-star evolution models. In particular, the type of supernova explosion that the star will undergo and

---

★ E-mail: awofford@astro.unam.mx

[1] S Doradus is one of the brightest stars in the LMC and one of the most luminous known. Its absolute V-band magnitude ranges from -7.6 (1969) to -10 (1989, van Genderen 2001). Stars with S Dor like variability are called S Doradus variables.

[2] Log($L/L_\odot$)∼ 5.4 to ∼ 6.4 (Vink 2012); extinction-corrected V-band absolute magnitude, $M_V \leq -7$ mag (Humphreys et al. 2014)

[3] For example, for Eta Carinae, $\dot{M} \sim 10^{-4}\,M_\odot\,\mathrm{yr}^{-1}$ during the quiescent phase and $\dot{M} \sim 10^{-2}\,M_\odot\,\mathrm{yr}^{-1}$ during the eruptive phase; (Humphreys & Davidson 1994).

[4] This is the MS lifetime of an $M_{ZAMS} \geq 40\,M_\odot$ star

the final mass of the remnant black hole or neutron star (if any) cannot be predicted. In fact, the mass loss during the LBV phase is one of the primary uncertainties in the classical formation channel for heavy binary black holes (e.g. Belczynski et al. 2016).

The lack of a complete LBV census prevents an accurate determination of the length of the LBV phase and the properties of stars in this unstable regime. Although cLBVs can be identified relatively quickly on the basis of their spectrum or luminosity, the identification of LBVs requires confirmation of the characteristic spectral and photometric variations. LBVs can be "quiescent" for decades or centuries during which they are indistinguishable from many other hot luminous stars. A key to understanding the peculiar instability of LBVs is their high observed luminosities, which often depend on uncertain distances. Much effort has been expended to identify new LBVs, with IR observations playing an important role in this regard. In particular, candidates have been identified via NIR spectroscopy and/or MIR imaging of circumstellar ejection nebulae (Clark et al. 2005, and references therein).

Table 1 summarizes the number of known Galactic and extra-galactic LBVs and cLBVs. The galaxies in which they are found sample a wide range of ionized-gas O/H ratios, i.e., 0.03 to 1.7 times the solar value. Trends between LBV properties and galaxy properties are difficult to investigate because i) bona-fide LBVs are incompletely characterized and ii) it is difficult to obtain multi-epoch spectroscopy for a sample of galaxies with a wide range of properties, at the spatial resolution which is necessary for such study.

Characterizing large samples of LBVs in different environments can provide valuable clues about their mass loss and evolution. Two *HST* programs, LEGUS (Legacy Extra-Galactic UV Survey, PID 13364, Calzetti et al. 2015) and Hα LEGUS (PID 13773, PI Chandar, Chandar et al., in prep.) offer a unique opportunity to search for cLBVs in new galaxies.

LEGUS is a Cycle 21 *HST* treasury program which obtained high spatial resolution ($\sim 0.07''$) images of portions of 50 nearby (≤ 16 Mpc) galaxies, using the UVIS channel of the Wide Field Camera Three (WFC3), and broad band filters F275W (2704 Å), F336W (3355 Å), F438W (4325 Å), F555W (5308 Å), and F814W (8024 Å), which roughly correspond to the photometric bands NUV, U, B, V, and I, respectively. The survey includes galaxies of different morphological types and spans a factor of $\sim 10^3$ in both star formation rate (SFR) and specific star formation rate (sSFR), $\sim 10^4$ in stellar mass ($\sim 10^7 - 10^{11}\,M_\odot$), and $\sim 10^2$ in oxygen abundance ($12 + \log O/H = 7.2 - 9.2$). Some of the targets in the survey have high quality archival images in bandpasses similar to those required by LEGUS, most of them from the Wide Field Channel of *HST*'s Advanced Camera for Surveys (ACS), and fewer of them, from ACS's High Resolution Channel (HRC). For the latter targets, LEGUS completed the five band coverage. The choice of filters was dictated by the desire to distinguish young massive bright stars from faint star clusters, to derive accurate star formation histories for the stars in the field from their CMDs, and to obtain extinction-corrected estimates of age and mass for the star clusters. Star and star-cluster catalogues have been released for the LEGUS sample and are described in Sabbi et al. (2018) and Adamo et al. (2017), respectively. We note

that the LEGUS data do not have the spatial resolution to visually resolve massive stars in close binary systems.

Hα LEGUS is a Cycle 22 program which obtained narrow-band, Hα (F657N) and medium band, continuum (F547M) images for the 25 LEGUS galaxies with the highest star formation rates, using the WFC3. The corresponding Hα observations reveal thousands of previously undetected H II regions, including those ionized by stellar clusters and "single" massive stars.

In this paper, we focus on NGC 7793, the nearest LEGUS galaxy of the Southern hemisphere. This galaxy was also observed by Hα LEGUS. Furthermore, we focus on the LEGUS field NGC 7793W, for which Adamo et al. recently secured ESO *VLT* MUSE (Bacon et al. 2010) spectroscopy with Adaptive Optics (AO) of two subfields (Della Bruna et al., subm.). We combine LEGUS and Hα LEGUS photometry with MUSE spectroscopy to search for cLBVs in NGC 7793W. Candidate LBVs are defined by Smith (2019) as stars with similar luminosities and spectra to LBVs, often with circumstellar shells that indicate a prior outburst, but which have not yet been observed photometrically to undergo LBV eruptions.

We start by using the *HST* photometry to create a catalogue of potential cLBVs (hereafter, photometric cLBVs). We then identify the photometric cLBVs which are located within the MUSE fields. Hereafter, we refer to the latter as MUSE cLBVs. Note that the latter are still potential cLBVs. This work focuses on the MUSE cLBVs. We proceed to check if the *HST* coordinates of the MUSE cLBVs are coincident with those of sources in other catalogues of the LEGUS collaboration, in particular: O-type stars (Lee et al. in prep.), compact star clusters (Hannon et al. 2019), star clusters (Adamo et al. 2017), and H II regions (Della Bruna et al., subm.). After this, we determine if the cLBV spectra are contaminated with light from nearby star clusters or H II regions. Finally, we spectroscopically classify the MUSE cLBVs and identify the most promising cLBVs.

In Section 2, we describe the galaxy and its imaging and spectroscopic observations. In section 3, we present our catalogue of photometric cLBVs. In Section 4, we check if our sources have matches in other LEGUS catalogues. In Section 5, we spectroscopically classify the MUSE cLBVs. In Section 6, we discuss our results. Finally, we summarize and conclude in Section 7.

2 SAMPLE AND OBSERVATIONS

2.1 NGC 7793

NGC 7793 is a SAd flocculent spiral, with an inclination of 47 degrees. It is the nearest Southern-hemisphere galaxy in LEGUS, and one of the brightest galaxies in the Sculptor Group. The main properties of the galaxy are: Cepheid-determined distance, 3.44 Mpc (Pietrzyński et al. 2010); color excess due to the Galaxy, $E(B - V) = 0.017$ mag (Schlafly & Finkbeiner 2011); stellar mass obtained from the extinction-corrected B-band luminosity and color information, using the method of Bothwell et al. 2009, based on the mass-to-light ratio models of Bell & de Jong (2001), $M_\star = 3 \times 10^9\,M_\odot$; galaxy-wide star formation rate calculated from the dust-attenuation corrected GALEX far-UV, adopting a distance of 3.44 Mpc, SFR=0.52 $M_\odot$ yr^{-1} (Lee et al.

Table 1. Census of LBVs or cLBVs in order of increasing distance.

Galaxy	Number			Distance		(O/H)/(O/H)$_\odot$		Ref[d]
	LBVs	cLBVs	Ref[a]	(Mpc)	Ref[b]	Value	Ref[c]	
Milky Way	19	42	(1)	-	-	1	(1)	(1)
LMC	8	19	(1)	0.04	(1)	(0.4)-0.5	(2,3)	(2)
SMC	2	2	(1)	0.04	(1)	0.23-(0.25)	(2,3)	(3)
NGC 6822	0	1	(1)	0.22-0.46	(2,3)	0.28	(3)	(4)
IC 1613	0	1	(1)	0.65	(3)	0.12	(3)	(5)
IC 10	0	3	(1)	0.74	(4)	0.37	(4)	(4)
M31	6	10-25	(1, 6)	0.74	(5)	1.05-1.7	(5)	(4, 6)
M33	5	28	(1)	0.9	(6)	0.47-0.79	(6)	(4, 6)
NGC 55	0	4	(2)	1.99	(4)	0.27-0.30	(7)	(2)
NGC 2403	2	1	(3)	2.5	(4)	0.61	(8)	(3)
NGC 2366	1	0	(1)	3.34	(4)	0.1	(9)	(7)
M81	0	2	(3)	3.55	(3)	0.27-2.5	(10)	(8)
M101	0	11	(4)	6.4	(3)	0.7-1.12	(11)	(4)
DDO 68	1	0	(5)	12.75	(7)	0.028	(12)	(9)
Total	44	124						

[a]Reference for the number of LBVs/cLBVs. Note that the confirmed LBVs are removed from the cLBV column. (1) Richardson & Mehner (2018). (2) Castro et al. (2008). (3) Humphreys et al. (2019). (4) Grammer et al. (2015). (5) Pustilnik et al. (2017). (6) King et al. (1998).

[b]Reference for the distance to the galaxy. (1) Groenewegen (2013). (2) Rich et al. (2014). (3) Freedman et al. (2001). (4) Tully et al. (2013). (5) Wagner-Kaiser et al. (2015). (6) Pellerin & Macri (2011).

[c]References for ionized-gas oxygen abundances, except for the Milky Way, which gives the ref. for the Solar photosphere value, which is $12+\log(O/H)=8.69$. (1) Asplund et al. (2009). (2) LMC/30 Doradus and SMC/N88A regions, Garnett et al. (1995) (values in parenthesis). (3) CEL values, Dopita et al. (2019). (4) IC 10, Magrini & Gonçalves (2009); Polles et al. (2019). (5) Central value of M31 (abundance gradient measured from 3.9 to 16.1 kpc of the centre: -0.023 ± 0.002 dex/kpc), Zurita & Bresolin (2012). (6) Inner 2 kpc of M33, Bresolin (2011). (7) Range of values obtained with different methods in NGC 55 Magrini et al. (2017). (8) Central value of NGC 2403 (abundance gradient: $(-0.032 \pm 0.007 \times R_g$ (dex kpc/1)), Berg et al. (2013). (9) NGC 2366/Mrk 71 Izotov et al. (2011). (10) Range given for M81 by Garnett & Shields (1987). Abundance gradient: -0.088 ± 0.013 dex kpc/1 (Stanghellini et al. 2014). (11) Central region of M101, Bresolin (2007). (12) Pustilnik et al. (2017).

[d]References with examples of photometry and/or spectra of LBVs/cLBVs. (1) Wolf & Stahl (1982); Miroshnichenko et al. (2014). (2) Walborn et al. (2017). (3) Koenigsberger et al. (2010). (4) Massey et al. (2007). (5) Herrero et al. (2010). (6) Humphreys et al. (2014). (7) Drissen et al. (2001). (8) Humphreys et al. (2019). (9) Pustilnik et al. (2017).

2009); SFR based on the integration of LEGUS fields NGC 7793W and NGC 7793E and averaged over the Hubble time (hence not directly comparable to the galaxy-wide UV measurement), calculated from CMD-fitting using F555W and F814W, adopting a distance of ~3.7 Mpc (Sabbi et al. 2018), SFR=0.23 ± 0.02 M$_\odot$/yr (Sacchi et al. 2019); central value of the oxygen abundance in the ionized gas, $12+\log(O/H) = 8.50 \pm 0.02$; and radial oxygen abundance gradient adopting a distance of 3.4 Mpc, -0.305 ± 0.048 dex R_{25}^{-1}, (Pilyugin et al. 2014).

2.2 *HST* imaging

Two fields of NGC 7793 (E and W), which have a small overlap, were observed as part of the LEGUS and Hα LEGUS programs. In this work, we focus on NGC 7793W, for which we recently obtained MUSE spectroscopy.

We retrieved the individual ACS and WFC3 flc images of NGC 7793W from the Mikulski Archive for Space Telescopes and initially processed them on-the-fly with CalACS version 8.2.1 (14-Nov-2013, LEGUS ACS data), CalWF3 version 3.1.4 (09-Sept-2013, LEGUS WFC3 data), and 3.1.6 (15-Nov-2013, Hα LEGUS WFC3 data). These images have gone through the following corrections: bias-shift, crosstalk, bias-stripe, charge transfer efficiency, dark. We then ran `As-`

`trodrizzle`[5] from `DrizzlePac` (STSCI Development Team 2012) on the flc images, one filter at a time. `Astrodrizzle` creates mask files for bad pixels and cosmic rays and drizzle-combines the input images using the mask files, while applying geometric distortion corrections, to create a "clean" distortion-free combined image. For our purposes, it was important to remove cosmic rays from the F658N and F547M flc files, prior to running dolphot.

In Table 2, we provide a summary of the LEGUS and Hα LEGUS observations. The left panel of Figure 1 shows a Digital Sky Survey (DSS) image of NGC 7793 with the WFC3 and ACS footprints overlaid. The right panel of Figure 1 shows an *HST* composite image of NGC 7793W with the *VLT* MUSE footprints overlaid.

2.3 MUSE spectroscopy

The MUSE data reduction is extensively presented in Della Bruna et al submitted. Here we provide a summary for the reader. NGC 7793W was observed on August 15th 2017 as part of the MUSE AO Science Verification run, with programme ID 60.A9188(A). The data were acquired in wide

---

[5] We used the following `Astrodrizzle` command: astrodrizzle.AstroDrizzle('i*flc.fits',output= 'ngc7793w_f657n',driz_sep_bits='64,32',driz_cr_corr=yes, final_bits='64,32',final_wcs=True,final_scale=0.05,final_rot=0.)

Table 2. Summary of *HST* observations of NGC 7793W. The F547M and F657N data are from the Hα LEGUS program (PI Chandar, PID 13773), and the rest from the LEGUS program (PI Calzetti, PID 13364). Note that the F657N filter is 94 Å wide and includes Hα + [N III].

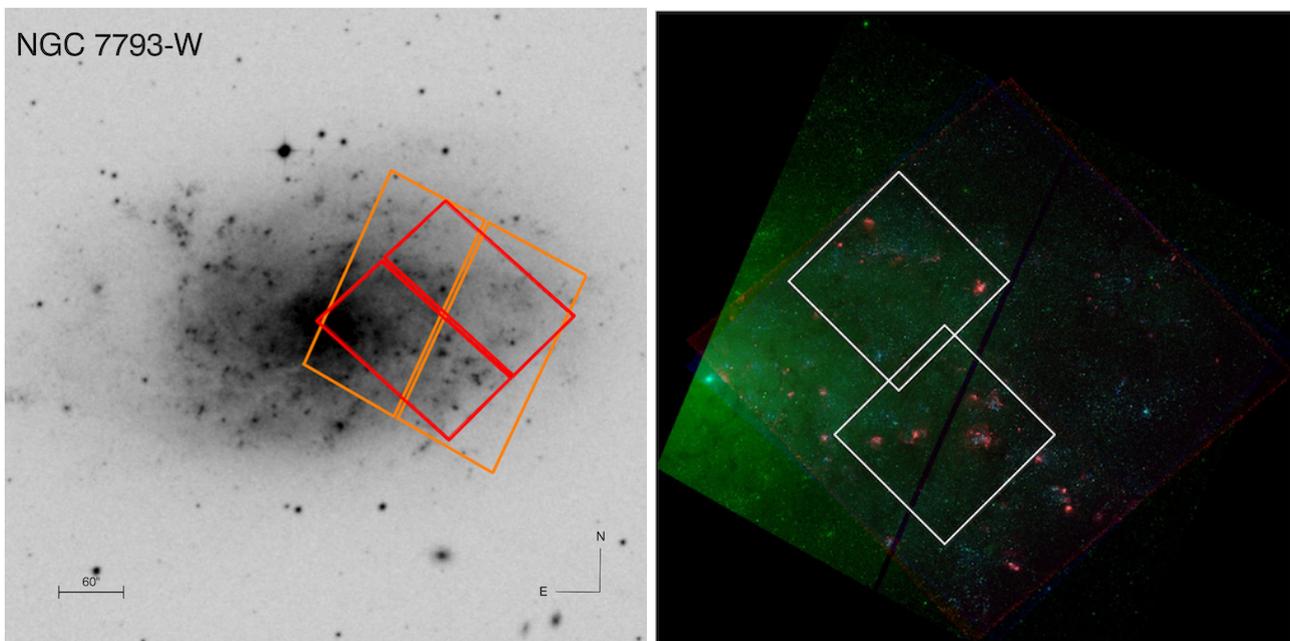| Instrument/Camera	Pixel Size (")	Field of View (")	Filter	Pivot Wavelength (Å)	Exposure Time (s)	Date Obs.
WFC3/UVIS	0.040	162 × 162	F275W	2710.1	2349.0	2014 Jan 18
			F336W	3354.8	1101.0 (367× 3)	2014 Jan 18
			F438W	4326.5	947.0	2014 Jan 18
			F547M	5447.4	550.0	2014 Dec. 07
			F657N	6566.6	1545.0 (515× 3)	2014 Dec. 07
ACS/WFC	0.05	202 × 202	F555W	5359.6	680.0 (340×2)	2003 Dec 10
			F814W	8059.8	430.0	2003 Dec 10

Figure 1. *Left.* DSS image of NGC 7793 with footprints of WFC3/UVIS and ACS/WFC *HST* observations of NGC 7793W overlaid (red and orange polygon, respectively). The image dimensions are 10'x10'. *Right.* Composite *HST* image of NGC 7793W (red, continuum subtracted F657N; green, F555W; and blue, F275W). We overlay the *VLT* MUSE footprints (white polygons), which have dimensions of 1'×1'.

field mode (WFM), with a 1 arcmin² FOV and a spatial resolution of 0.2 arcsec, and over the extended wavelength range 4650 – 9300 Å, sampled in steps of 1.25Å. The spectral resolution of the MUSE spectra is *FWHM* ~ 2.6 Å at 4650 Å and *FWHM* ~ 2.5 Å at 9300 Å. The two MUSE pointings are centred at RA & Dec coordinates (23:57:42.3070, -32:35:48.150) and (23:57:43.8894,-32:34:49.353).

Four exposures (each rotated 90 degrees with respect to the previous one), with a total of 2100 s on source, were acquired for each pointing. As the target fills the entire MUSE field of view, separate sky frames of 120 s exposure were also acquired in between science exposures (in an object-sky-object sequence).

The data were reduced with the MUSE ESO pipeline (Weilbacher et al. 2014, v2.2), which performs standard calibrations (bias subtraction, flat fielding, wavelength- and flux-calibrations) as well as sky subtraction. The sky model is constructed on the separate sky frames by running the `muse_create_sky` task, and then subtracted from the science frame using the 'subtract-model' option in

`muse_scipost`. The absolute astrometry of the resulting datacube is matched to the HST LEGUS observations (Calzetti et al. 2015). On the final cube, we measure a seeing of 0.71" full-width at half-maximum at 4900 Å.

For extracting the spectra of the individual photometric cLBVs, we use the `astropy` library of `python`, and an extraction diameter of 4 pixels or 0.8", i.e., slightly larger than the seeing of the MUSE observations.

In Figure 2, we show an example of a cLBV MUSE spectrum with the system throughput curves of filters used in this work, overlaid.

3 CATALOGUE OF PHOTOMETRIC CLBVS

We expect cLBVs to have strong Balmer lines (particularly Hα, e.g., King et al. 1998). Such lines can have P-Cygni profiles or be in pure emission if the P-Cygni absorption component is filled in by nebular emission (e.g., Grammer et al. 2015). King et al. (1998) found an efficient method to iden-
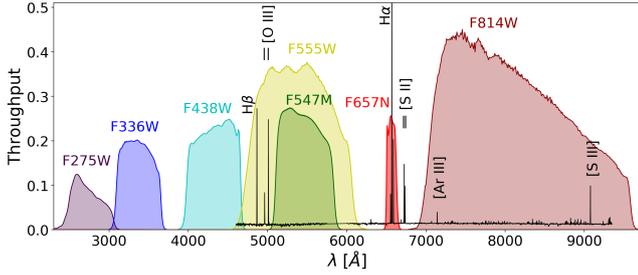
Figure 2. System throughput curves of the seven filters which were used in this work (see Table 2). In order to show which strong emission lines are present in the band passes of the filters, we overlay the MUSE spectrum of photometric cLBV #9 in arbitrary flux units. The F814W filter includes the hydrogen Paschen series.

tify cLBVs in nearby galaxies, based on deep, continuum-subtracted narrow-band Hα and [S II] images. The cLBVs were selected as objects with extremely low [S II]/Hα ratios and with coincident stellar objects in continuum images. Five of their most promising candidates identified by these criteria in M31 were subsequently confirmed by optical spectroscopy to show spectra similar to the previously identified M31 LBV, HS var 15. The latter five candidates also have much in common with B[e] stars.

In this work, we select potential cLBVs by combining images in the F547M, F657N and F814W filters, with restrictions of roundness, sharpness and Hα luminosity. In this section, we describe in detail how we select our sample of potential cLBVs.

3.1 Methodology.

Positions and fluxes for point-like sources were measured via PSF-fitting using the WFC3 and ACS modules of the photometry package dolphot version 2.0, downloaded on 2014 December 12 from the website http://americano.dolphinsim.com/dolphot/.

dolphot is a stellar photometry package that was adapted from HSTphot for general use. We performed the stellar photometry on the flc images with the cosmic rays flagged. In order to run dolphot we used a custom python script which was developed by co-author L. U.. Dolphot was run separately for the five LEGUS filters (F275W, F336W, F438W, F555W, F814W) and the two Hα LEGUS filters (F547M and F657N). The steps followed to find the cLBVs follow.

i) Select sources from the dolphot output with a signal-to-noise ratio (SNR) > 4 in filters F547M and F657N, and in the intersection of sharpness = [-0.03 to 0.02] and roundness = [0.0 to 0.4]. This avoids selecting larger objects like compact clusters and non-localized Hα emission.

ii) Run TOPCAT (Taylor 2011) to find the intersection between F547M, F657N, and F814W point sources using a 2-dimensional Cartesian search, such that the error in the distance between sources is less than 0.5 pixels[6].

iii) Remove sources which are within 3 pixels from the edges of the images using a routine developed by co-author D. T.

iv) Use the F547M and F814W images to determine the continuum and subtract it from the F657N image, for each cLBV. Compute the continuum subtracted Hα luminosity. For the previous two steps we used a routine developed by co-author J. L..

v) Select all remaining sources with an Hα luminosity of $\log(L(\text{H}\alpha) \text{ [erg s}^{-1}\text{]}) \geq 35$, which is the 5-$\sigma$ detection threshold for a point source.

Following these steps, we find ~100 potential cLBVs (hereafter, less conservative approach). We can also apply a more conservative approach by requiring in step (ii) a SNR>4 in all five LEGUS and two Hα-LEGUS filters, which yields 76 potential cLBVs. In Figure 3, we compare the samples of potential cLBVs obtained with the conservative approach (left panel) and less-conservative approach (right panel) in magnitude-color diagrams. We show F547M-F657N, where F657N is not continuum subtracted, on the y-axis, and F657N$_{\text{line}}$, which is continuum-subtracted, on the x-axis. In both panels, sources which are 5-σ above the Hα detection threshold for a point source are located to the left of the vertical dashed line. The top cloud of unfilled circles in the right panel (which is not present in the left panel) corresponds to sources with non-detections in the UV, U, and/or B filters. In this work, we adopt the less conservative approach and call the potential cLBVs selected via the less conservative approach, photometric cLBVs.

Since the selection was not performed using the LEGUS stellar catalogues, we compare our catalogue of photometric cLBVs against the v2 stellar catalogue of Sabbi et al. (2018). All photometric cLBVs have matches in the catalogue of Sabbi et al. (2018). In addition, by comparing the F555W-band magnitudes of Sabbi et al. (2018) and this work, we find mean and median percent errors of 0.02 and 0.005, for the entire sample of photometric cLBVs, respectively[7]. This indicates that the magnitudes from both catalogues are in very good agreement.

A cLBV must have spectroscopic similarities with bona-fide LBVs. Thirty six of the photometric cLBVs fall in the MUSE fields. The MUSE cLBVs are shown with red squares in Figure 3. The latter figure shows that the Hα-brightest photometric cLBVs are outside of the MUSE field of view.

3.2 Color-color diagrams

Figure 4 shows the color-color (CCD) diagram, F438W − F555W versus F555W − F814W of our candidate LBVs. The color bar shows the Hα luminosity. The right panel of the figure, which is an enlargement of the blue portion of the CCD on the left, shows that two of the most α luminous cLBVs are located in bluest part of the CCD.

---

[6] For the relevant datasets, 0.5 pixels is the typical distance error between points which are the same source in different *HST* images.

[7] The percent errors were computed as follows: absolute value of ((F555W$_{\text{Sabbi}}$ - F555W$_{\text{ThisWork}}$) / F555W$_{\text{Sabbi}}$)×100, where F555W is the apparent magnitude.
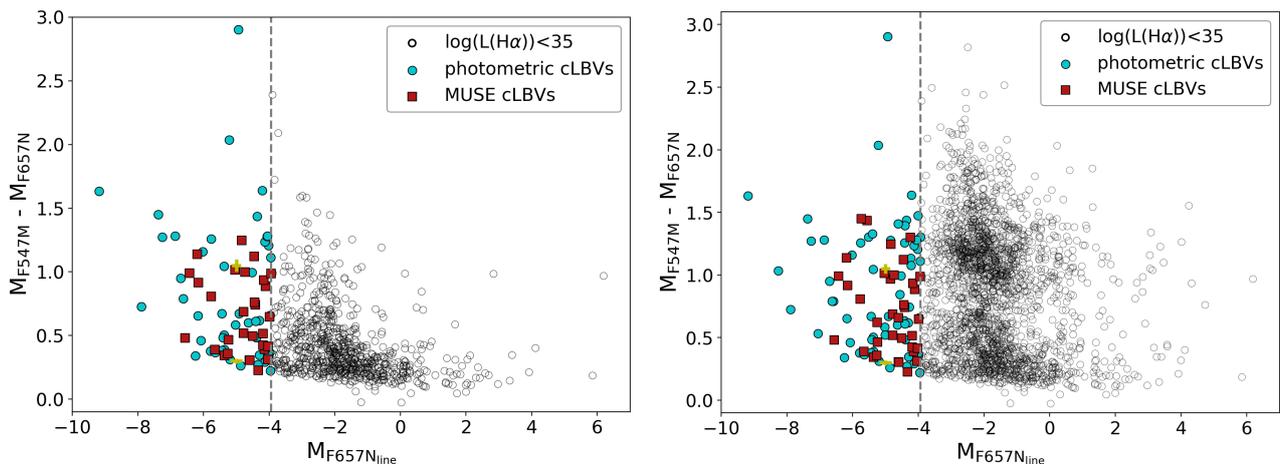
Figure 3. *Left.* F547M − F657N color versus continuum-subtracted F657N absolute magnitude for sources selected via the conservative approach (all magnitudes are extinction uncorrected). The black unfilled circles are sources with lower Hα luminosities than the photometric cLBVs. We mark with a vertical dashed line the minimum Hα luminosity of the cLBVs. The filled circles are the photometric cLBVs which are outside of the MUSE fields. The filled squares are the MUSE cLBVs. We show two mean photometric error bars in yellow for points around (-5, 0.25) and (-5, 1), where the first and second numbers are the absolute magnitude in F547M and F547M − F657N. *Right.* Similar to the left panel but we use the less conservative approach, which is the one adopted in this work.
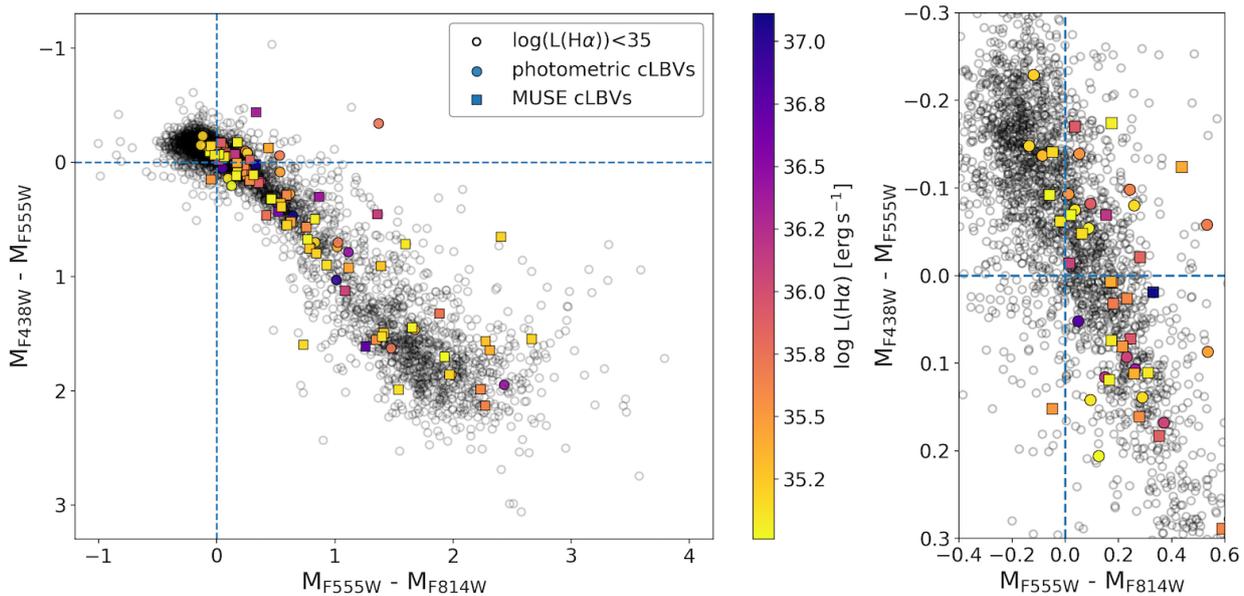

Figure 4. *Left.* F438W − F555W versus F555W − F814W color-color diagram for sources which are selected via the less conservative approach. We plot absolute magnitudes uncorrected for extinction. Not included in this diagram are the photometric cLBVs which are undetected in F438W, F555W and/or F814W; i.e. four photometric cLBVs without MUSE coverage and two MUSE cLBVs. The blue dashed lines mark the positions of zero color in the x and y directions. *Right.* Enlargement of the upper left region of the plot in the left panel.

3.3 Extinction due to dust

For massive stars, the standard procedure to correct for extinction due to dust intrinsic to the galaxy is to fit a stellar atmosphere model to the observed stellar spectrum in order to find the intrinsic spectrum of the star. It is by comparing the intrinsic spectrum to the observation that one finds the value of the extinction. It is beyond our goal to fit stellar atmosphere models to the MUSE cLBVs and find the intrinsic

extinction using this method. Thus, we do not correct the observations for intrinsic extinction. As shown in Section 5, this does not prevent us from finding promising cLBVs in this work. In Table A1 of the appendix, we provide the extinction un-corrected photometry of the MUSE cLBVs. Note that Kahre et al. (2018) provide extinction maps for NGC 7793W. Their extinctions span a range between A(V) = 0 − 1 peaking around 0.5 mag.

3.4   V-band magnitude

An object more luminous than $M_V \sim -7.0$ is unusual and therefore a good LBV candidate. However, the latter objects can also be hypergiants (Clark et al. 2012). After the extinction correction, the confirmed LBVs in M31 and M33 have $M_V \leq -7$ (Humphreys et al. 2014). We found 24 photometric cLBVs with extinction-uncorrected V-band magnitudes such that, $M_V \leq -7$. These would be even brighter after the extinction correction. Unfortunately, only seven of these are in the MUSE fields, as summarized in Table 3, where column 1 gives the ID of the MUSE cLBV and column 2 gives the extinction-uncorrected V-band magnitude. In Table 3, the MUSE cLBVs are sorted in order of decreasing luminosity (most luminous at the top). Since the brightest "normal" blue supergiant stars are at $M_V \sim -6.0$ or slightly brighter, it is likely that most objects with such magnitudes are normal supergiants. All sources in Table 3 are spectroscopically classified as described Section 2.3.

3.5   Color-magnitude diagrams

We looked at the CMD positions of our photometric cLBVs relative to the bona-fide LBVs of M33 which are plotted in figure 5 of Clark et al. (2012). The result is shown in Figure 5, where we put our cLBVs at the distance of M33, i.e., 964 kpc (Clark et al. 2012). We overlay PARSEC v1.2S stellar tracks (Bressan et al. 2012; Tang et al. 2014) for various initial stellar masses, a metallicity of $Z = 0.005$, and a Salpeter Initial Mass Function, using the photometric system of Maíz Apellániz (2006) and Bessell (1990). We attribute the spread of the photometric cLBVs in the diagrams to a combination of extinction and evolutionary phase. The MUSE cLBVs with IDs 1 to 7, i.e., the ones with $M_V \leq -7$, fall in the region of M33 LBVs. In conclusion, our method for finding potential cLBVs via an Hα excess works. We note that a few of the sources with $\log(L(H\alpha))<35$ (black open circles) are also close to the bona-fide LBVs of M33 in Figure 5. This is due to the arbitrary cut at $\log(L(H\alpha))<35$.

4   MATCHES WITH SOURCES IN LEGUS CATALOGUES

Prior to the spectral classification of the MUSE cLBVs, we check if their *HST* coordinates match those of other types of sources which are identified in the following LEGUS-collaboration catalogues: candidate O-type stars identified via LEGUS photometry (Lee et al., preliminary catalogue; star clusters of less than 10 Myr classified according to *HST* Hα morphology (Hannon et al. 2019); star clusters identified via LEGUS photometry (Adamo et al. 2017); and H II regions identified via two-dimensional MUSE spectroscopy (Della Bruna et al., subm.). We also look for members of the above catalogues which are located within the radius used for the spectral extraction and which contaminate the cLBV spectra.

4.1   Search radii

The coordinates of a given source in the different *HST* images can be off by a distance of up to 0.5 pix or 0.02", which

at a distance of 3.44 Mpc yields 0.3 pc. We use 0.5 pix as the search radius to find matches between the coordinates of the MUSE cLBVs and candidate O-type stars. The radius used to extract the photometry of LEGUS star clusters in NGC 7793 is 5 pix or 0.2" (3 pc). We use 5 pix as the search radius to find matches between MUSE cLBVs and star clusters. The comparison is performed with TOPCAT. The seeing of the MUSE observations is 0.8". We use 0.4" as the search radius to find contaminants to the cLBV spectra.

4.2   Candidate O-type stars

In their preliminary catalogue, Lee et al. (in prep.) identify candidate main sequence O-stars ($M \geq 20 M_\odot$) by their positions in color-magnitude (I vs B-I) and Q-magnitude (reddening-free index computed from NUV, B, I photometry vs I) diagrams. The definition of Q is given in Johnson & Morgan (1953). Lee et al. use simulated HST photometry which is generated using stellar evolutionary tracks along with assumptions on the IMF, star formation history, and dust attenuation, to estimate the completeness and contamination rates, and to optimize the selection. The photometry incorporates accurate photometric errors based on artificial star tests. With the simulated photometry, they examine their selection based on the 6 three-filter combinations that include the bluest filter available (NUV: F275W), as well as the standard UBV set for reference. They find that the yield is maximized with NUV, B, and I photometry, with estimated completeness of $\sim$70% and contamination rate of $\sim$30%. Comparing against their catalogue, we find one candidate O-type star per MUSE cLBV within the search radius of 0.02", i.e., all MUSE cLBVs are also classified as candidate O-type stars. In addition, we find several candidate O-type star contaminants per cLBV, i.e., beyond 0.02" and within a search radius of 0.4", as summarized in column 6 of Table 3.

4.3   Star clusters classified by Hα morphology

Hannon et al. (2019) use the H$\alpha-$ LEGUS images of three galaxies, including NGC 7793 to classify star-clusters younger than 10 Myr according to their H-alpha morphology. They use the classification scheme of Hollyhead et al. (2015), who defined three classes based on the presence and shape of the Hα emission, which is similar to that of Whitmore et al. (2011): 1) concentrated, where the target star cluster has a compact H II region and where there are no discernable bubbles or areas around the cluster which lack Hα emission (these are expected to be about 3 Myr old); 2) partially exposed, where the target cluster shows bubble like/filamentary morphology covering part of the cluster; and 3) no emission, where the target cluster does not appear to be associated with Hα emission. We check the overlap between our MUSE cLBVs and the concentrated clusters of Hannon et al. (2019). We find no matches with concentrated clusters within a radius of 0.2", but we do find 5 matches with clusters of morphological type 2 and 3 within that radius. In addition, we find that no concentrated clusters contaminate the spectra of the MUSE cLBVs, although some clusters of morphological type 2 and 3 do contaminate them. This is summarized in columns 7 and 8 of Table 3, which give the morphological type of the star clusters found
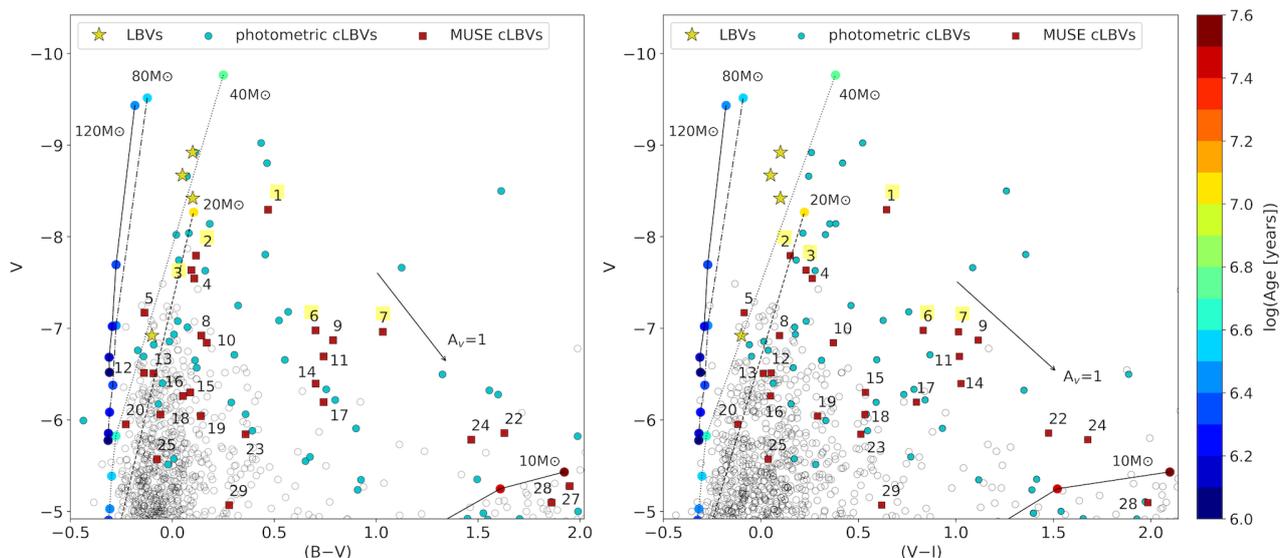
Figure 5. Color magnitude diagrams adapted from Clark et al. (2012). The four yellow stars are bona-fide M33 LBVs, whose V-band magnitudes are provided at the bottom of table 1 of Clark et al. (2012). To convert to absolute magnitudes we use a distance modulus, μ=24.92 (Bonanos et al. 2006). We overlay our photometric and MUSE cLBVs at the distance of M33. The cyan filled circles represent photometric cLBVs outside of the MUSE fields. The red squares represent MUSE cLBVs. The black unfilled circles represent sources with the same selection criteria as the photometric cLBVs but with lower Hα luminosities. The IDs of the five strongest cLBVs are highlighted in yellow. We overlay Padova tracks for various initial stellar masses and a metallicity of $Z = 0.005$ (see text for more details). Circles of different colors along the tracks correspond to the stellar ages (years) in logarithmic scale which are given in the colorbar. *Left.* F438W (B) - F555W (V) versus F555W. *Right.* F555W - F814 (I) versus F555W. The arrow represents the extinction vector corresponding to A(V)=1.

within a radius of 0.2" form the MUSE cLBVs. The additional clusters found within a radius of 0.4" are marked with asterisk. Note that two independent sets of evolutionary tracks, Padova and Geneva, were used in Hannon et al. (2019) to find clusters with ages of less than 10 Myr. These yield slightly different numbers of such clusters, which explains the case of cLBV #27, with no matching clusters according to Padova and one matching cluster according to Geneva.

4.4   Star clusters

Adamo et al. (2017) produced comprehensive high-level young star cluster (YSC) catalogues for a significant fraction of LEGUS galaxies, including NGC 7793. For the cluster catalogues, Adamo et al. (2017) perform a visual inspection in order to minimize contaminants in their final catalogues and add missed clusters. The total number of clusters which were visually classified in NGC 7793W is 299. Of the latter, 135 sources were classified as compact star clusters (Class 1 and 2, Kim et al. in prep). The NGC 7793 catalogues have been used by Krumholz et al. (2015) to determine the ages, masses, and extinctions of clusters in NGC 7793 using cluster-SLUGS; Grasha et al. (2017) to investigate the hierarchical clustering of the YSCs; Grasha et al. (2018) to study the relationship between giant molecular cloud properties and the associated star clusters; and Hannon et al. (2019) to study the Hα morphology of star clusters. The LEGUS cluster catalogues can be found here: https://archive.stsci.edu/prepds/legus/dataproducts-public.html.

   We find 11 matches between the MUSE cLBVs and star

clusters within a radius of 0.2" and three additional cases where clusters are located within a radius of 0.4", i.e., contaminate the cLBV spectra. In Table 3, columns 9 and 10 give the ages of the matching/contaminating star clusters, where the additional clusters found within a radius of 0.4" are marked with asterisk. Those ages are based on two different sets of solar-metallicity stellar evolution tracks (as no other metallicity is currently available for NGC 7793). We remind the reader that according to single-star evolution, clusters of ~5 Myr and older are too old to host LBV stars. Seven of the twelve contaminating star clusters are 5 Myr or older. As will be shown in the next section, the rest of the contaminating clusters are around cLBVs with signatures of the presence of W-R stars. Interestingly, Table 3 shows that six of the candidates with $M_V \le -7$ have no contaminating star clusters. This is discussed in the context of the binary formation scenario of LBVs in section 6.1.

4.5   H II regions

The H II region selection is presented in Della Bruna et al. (subm.). We provide below a concise description. Della Bruna et al. identify H II regions by constructing a hierarchical tree structure on the MUSE Hα flux map. To do this, they use the python package ASTRODENDRO[8]. As input data for the algorithm, they use a flux map obtained by integration of the continuum-subtracted cube in the rest frame wavelength range $6559 - 6568$ Å. They assume a Gaussian

---

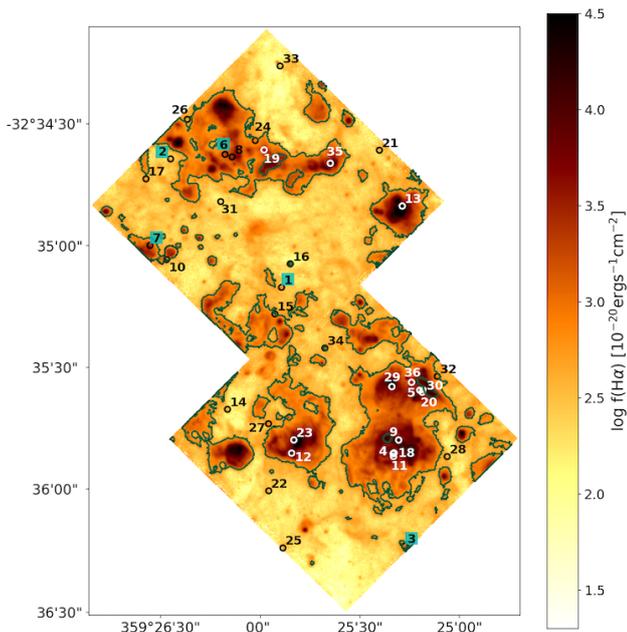[8] Hierarchical tree structure visual explanation under https://dendrograms.readthedocs.io

Figure 6. MUSE continuum-subtracted Hα emission map with positions of MUSE cLBVs indicated with circles with IDs. The IDs of the five strongest cLBVs are highlighted in cyan. The green contours show the H II regions from the catalogue of Della Bruna et al. (subm.). Each of the two MUSE fields is 1'×1' on the side. At the adopted distance of 3.44 Mpc, 60" represent ~1 kpc.

background for the diffuse Hα radiation and compute the hierarchical tree down to 10 sigma above the background mean. They select all leaves of the structure and also the branches that enclose the largest H II regions, inside of which the algorithm identifies resolved sub-peaks as distinct leaves. Therefore, they do not use any fixed aperture to define the H II regions. They also look at BPT (Baldwin et al. 1981) diagrams ([S II]/Hα and [N II]/Hα) to assess that the candidate regions are consistent with being photoionized and to exclude potential contaminants (e.g planetary nebulae and supernova remnants).

In Figure 6, we show the H II regions map of Della Bruna et al.. We overlay and identify our 36 MUSE cLBVs. We include MUSE cLBVs which are located at the edges of the Hα map because their MUSE spectra do not seem to suffer from any artifacts. We visually check if the MUSE cLBVs are located within H II-region contours in Figure 6 and find 22 MUSE cLBVs where this is the case. Column 11 of Table 3 summarizes these results.

Candidates #1 and #2 are located outside H II regions and candidate #3 is in a small H II region which is isolated from the large H II region complexes which are shown in Figures 6 and 1. The *HST* postage stamps of the latter cLBVs are shown in Figure 7, which confirms the findings just described.

5   SPECTRAL CLASSIFICATION OF MUSE CLBVS

Here we discuss the spectral classification of the 36 potential cLBVs in the MUSE fields. For all MUSE cLBVs, Figures 7,

8, 9, and 10, show postage stamps and optical spectra in spectral windows of interest. The IDs of the candidates are given in the upper-right corner of the postage stamps. In Figures 7, 8, and 9, we skip the MUSE cLBVs which show broad He II λ4686 emission. The latter sources are shown in the last seven rows of Figure 10 and discussed in the context of W-R stars. For each MUSE cLBV, Table 4 provides a summary of the spectroscopic measurements which we discuss in this section.

5.1   Most promising MUSE cLBVs

There is no consensus on how to spectroscopically classify an object as a candidate LBV. In general, candidate LBVs show strong Balmer and/or optical He I emission lines, typically (but not always) with P-Cygni like profiles. The appearance is not unlike what we see in some Type IIn supernovae, with narrow Balmer emission atop a broader base (King et al. 1998).

As previously shown, candidates LBVs #1 to #7 have photometric properties which are compatible with known properties of LBVs. Among the latter, only candidate #2 shows Hα with a P-Cygni like profile. The profile is shown in Figure 11. The other strong candidates show Hα in pure emission.

The spectral resolution of the MUSE observations in the Hα region is $FWHM \sim 120\,\mathrm{km\,s^{-1}}$. We do not detect a broad Hα component in emission for cLBVs #1 to #7. For cLBVs, typical values of the full width at half maximum ($FWHM$) for the narrow component of Hα are in the range $100-200\,\mathrm{km\,s^{-1}}$ (Humphreys et al. 2017a). We measure the $FWHM$(Hα) values of the MUSE candidates. For this purpose, we fit one or more Gaussians to Hα, depending on the presence of components in broad emission and/or absorption. The results are shown in column (2) of Table 4. We find values between 119 and 155 km s^{-1}, as shown in the min and max rows of column (2). Only the sources with values above 120 km s^{-1} are resolved. The latter sources are within the upper limit of the expected range.

Unfortunately, the strongest He I line in the optical, He I λ5876, falls in the AO laser gap of the MUSE observations and thus was not observed. For this reason, we look at He I λ6678. As shown in column 3 of Table 4, among MUSE cLBVs #1 to #7, He I λ6678 emission is only observed from #4 and #5. The He I λ6678 line is shown as an inset in the rightmost panel of Figures 7 to 10.

Candidate LBVs may also show optical emission lines or P-Cygni like profiles of Fe II and Fe III and are generally distinguished by these "unusual" features from other Hα-bright objects. Examples of these lines in cLBVs can be seen in Castro et al. (2008). We attempted to remove the background light from the spectra of the candidates to see if we could detect faint features in their spectra. For this purpose, we computed the background from a ring around the candidate, which had an inner radius equal to 3/2 times sigma, where sigma is the standard deviation of the Gaussian which we fitted to the radial profile of the candidate's MUSE continuum-subtracted Hα emission. The ring had a width of one pixel. We found the median spectrum of all pixels within the ring and multiplied it by the number of pixels within the area of extraction of the cLBV spectrum. Background subtraction using this method was difficult because

Table 3. Photometric properties of MUSE cLBVs.

ID	RA[a]	Dec[a]	M_V^b	L(Hα)[c]	O[d]	CC[e]		SC[f]		H II[g]
						Padova	Geneva	Padova	Geneva	
(1)	(2)	(3)	(4)	(5)	(6)	(7)	(8)	(9)	(10	(11)
1	23:57:43.617	-32:35:10.691	-8.29±0.05	36.06±0.03	8	0	0	0	0	0
2	23:57:45.821	-32:34:38.168	-7.79±0.05	35.58±0.05	8	0	0	0	0	0
3	23:57:41.170	-32:36:16.184	-7.64±0.05	35.90±0.03	7	0	0	0	0	1
4	23:57:41.400	-32:35:52.769	-7.54±0.05	35.09±0.11	16	2, 2*	2, 2*	4, 2*	3, 2*	1
5	23:57:40.872	-32:35:36.706	-7.17±0.05	35.38±0.05	10	0	0	0	0	1
6	23:57:44.739	-32:34:37.020	-6.98±0.05	35.54±0.06	13	0	0	0	0	1
7	23:57:46.228	-32:35:00.058	-6.96±0.05	35.70±0.04	17	0	0	0	0	1
8	23:57:44.600	-32:34:37.653	-6.92±0.05	35.11±0.13	10	3	3	5	5	1
9	23:57:41.292	-32:35:49.332	-6.87±0.05	35.66±0.04	15	0	0	5*	5*	1
10	23:57:45.899	-32:35:03.626	-6.84±0.05	35.17±0.10	8	0	0	0	0	1
11	23:57:41.394	-32:35:53.490	-6.69±0.05	35.73±0.03	11	0	0	600	700	1
12	23:57:43.416	-32:35:52.641	-6.51±0.05*	35.91±0.03	11	0	0	0	0	1
13	23:57:41.221	-32:34:50.083	-6.51±0.05	35.74±0.04	21	0	0	0	0	1
14	23:57:44.690	-32:35:41.549	-6.40±0.05*	35.22±0.09	27	0	0	200	200	0
15	23:57:43.749	-32:35:17.408	-6.30±0.05	36.01±0.03	8	0	0	200	200	1
16	23:57:43.442	-32:35:04.726	-6.26±0.05	35.05±0.13	10	0	0	0	0	1
17	23:57:46.308	-32:34:43.224	-6.19±0.05	35.53±0.05	11	0	0	0	0	0
18	23:57:41.383	-32:35:52.587	-6.06±0.05	35.11±0.07	17	2, 2*	2, 2*	2,4*	2, 3*	1
19	23:57:43.964	-32:34:35.874	-6.04±0.05	35.20±0.12	8	0	0	0	0	1
20	23:57:40.823	-32:35:37.211	-5.95±0.05	35.21±0.06	24	3	3	3	3	1
21	23:57:41.672	-32:34:35.971	-5.87±0.05	35.28±0.07	5	0	0	0	0	0
22	23:57:43.872	-32:36:02.178	-5.86±0.05	35.05±0.08	9	0	0	0	0	0
23	23:57:43.373	-32:35:49.305	-5.84±0.05	35.13±0.08	6	0	0	300	3000	1
24	23:57:44.138	-32:34:33.512	-5.78±0.05	35.27±0.08	12	0	0	0	0	1
25	23:57:43.589	-32:36:16.642	-5.57±0.05	35.45±0.04	11	0	0	0	0	0
26	23:57:45.487	-32:34:28.146	-5.34±0.05	35.35±0.07	9	0	0	0	0	0
27	23:57:43.878	-32:35:45.186	-5.28±0.05	35.54±0.03	14	0	3	3000	7	0
28	23:57:40.328	-32:35:53.519	-5.10±0.05	35.03±0.07	5	0	0	0	0	0
29	23:57:41.425	-32:35:35.809	-5.07±0.05	35.33±0.04	9	0	0	5	4	1
30	23:57:40.812	-32:35:36.533	-4.88±0.05	35.37±0.04	14	0	0	1	2	1
31	23:57:44.825	-32:34:48.969	-4.70±0.05	35.24±0.07	10	0	0	0	0	0
32	23:57:40.525	-32:35:33.206	-4.63±0.05	35.08±0.06	11	0	0	0	0	1
33	23:57:43.647	-32:34:14.648	-4.43±0.05	35.28±0.07	7	0	0	0	0	0
34	23:57:42.755	-32:35:26.029	-4.20±0.06	35.01±0.06	9	0	0	0	0	1
35	23:57:42.648	-32:34:39.271	-4.01±0.06	35.35±0.06	11	0	0	0	0	1
36	23:57:41.036	-32:35:34.696	-3.42±0.06	35.10±0.05	5	0	0	0	0	1

[a] J2000 coordinate in LEGUS WFC3/UVIS/F657N image. RA=Right ascension in format hours:minutes:seconds. Dec=declination in format degrees:minutes:seconds.

[b] Absolute F555W magnitude in ascending order (most luminous at the top). The two cases where the source is undetected in F555W but is detected in F547M are marked with asterisks in the column. In those cases, we give the F547M value. The error in the absolute magnitude includes the photometric and distance modulus error. The error in the distance modulus is 27.68 ± 0.05 mag (Pietrzyński et al. 2010).

[c] Hα luminosity in erg s^{-1} (uncorrected for reddening), in logarithmic scale, calculated from the PSF-photometry. The error in the luminosity includes the photometric and distance modulus errors. The F657N filter includes the [N II] lines.

[d] Number of candidate O-type stars within a radius of 0.4", including the candidate within a radius of 0.02".

[e] Morphological type of contaminating star cluster as defined by Hannon et al. 2019 (2=partially exposed. 3=no Hα). Only clusters with ages of 10 Myr according to the Padova or Geneva models are considered in Hannon et al. (2019). Asterisk= clusters within a radius of 0.4" of the cLBV and outside a radius of 0.2".

[f] Ages (in Myr) of contaminating star clusters in the catalogue of Adamo et al. (2017), based on the Padova or Geneva models. Asterisk= star clusters within a radius of 0.4" of the cLBV and outside a radius of 0.2".

[g] Contamination by H II regions. 1=MUSE cLBV is within an H II region contour. 0=MUSE cLBV is not within an H II region counter (see text for more details).

the surrounding light is spatially inhomogeneous and can be brighter than the cLBV continuum. In the end, we decided not to do a background subtraction, except for sources #1 through #7, where there is not much evidence for Hα contamination from the surrounding area, and which seem dominated by very local emission line spectra. We detect no Fe lines in the spectra of candidates #1 to #7, even after subtracting the nearby light from the background in order to see fainter features.

Humphreys et al. (2017a) recently published a comparison of luminous stars in M31 and M33 and how to tell them apart. According to their research, confirmed LBVs: i) do not have [O I]λ6300 emission lines in their spectra; ii) have [Fe II] emission lines sometimes; iii) show free-free emission in the near-infrared but no evidence for warm dust; and iv)

show S Dor-type variability (this is the most important and defining characteristic). As can be seen in column 5 of Table 4, only candidates #4 and #5 show [O I]λ6300 emission in their spectra. As shown in column 4 of the same table, these two same candidates show He II emission. Hereafter, we exclude cLBVs #4 and #5 from our list of strong MUSE cLBVs.

Humphreys et al. (2017a) also say that cLBVs should share the spectral characteristics of confirmed LBVs with low outflow velocities (measured from the absorption component of the P-Cygni profile) and the lack of warm circumstellar dust (excess at 3.5 and 8 microns reveal the presence of warm circumstellar dust). Luminous Blue Variables are well known to have low wind speeds of 100 to 200 $km\,s^{-1}$ during their eruptions or maximum light phase and LBVs in quiescence are typically 50 to 100 $km\,s^{-1}$. Candidate LBV #2 has a P-Cygni profile in Hα with a an absorption minimum which is blueshifted by 222 $km\,s^{-1}$. We do not have either infrared data at the required spatial resolution to check for the lack of circumstellar dust. For something to be classified as an LBV, some people also require that there is an Hα+[N II] shell nebula, which is suggestive of a previous giant eruption. We do not have the spatial resolution to observe such shell.

Smith et al. (1998) used the Faint Object Spectrograph on *HST* to study the nebulae around the known LBVs, R127 and S119, in the LMC. The spectra of these nebulae show strong [N II], possibly due to N enrichment, relative to H II regions, and that the electron density is high, with the [S II]6716/[S II]6731 ratio near ∼ 1. We measured this ratio for the MUSE cLBVs.

Another characteristic of LBVs is that their [O III] λ5007 is generally low relative to that of H II regions. In order to use this fact as a tracer of cLBVs, one has of course to consider the metallicity gradient of the galaxy being studied and that presumably, the [O III] λ5007 strength varies as the star cycles between hot and cooler phases.

We report our measurements of the line flux ratios, [O III] λ5007/Hβ, [N II]6584/Hα, and [S II]6716/[S II]6731 in columns 6, 7, and 8 of Table 4. The last three rows of the table give the mean, median and standard deviation around the mean computed from the values of the entire column. The last column of Table 3 shows that about 2/3 of the MUSE cLBVs have spectra which are contaminated by H II regions. Figure 7 and column 6 of Table 4 show that cLBVs #1, #2, #3, #6, and #7 have weak or no [O III] λ5007 emission relative to the mean of the column. Column 7 of Table 4 shows that cLBVs #1 and #2 have above average [N II]6584/Hα ratios relative to the 36 MUSE cLBVs. This is consistent with the N-enriched shells around LBVs. Finally, column 8 of Table 4 shows that cLBVs #1 and #2 have below average [S II]6716/[S II]6731 ratios of 1.22 and 1.11, respectively, similar to the shells studied by Smith et al. (1998). In summary, we have found five strong cLBVs (#1, #2, #3, #6, and #7) among which #1 and #2 are the strongest.

5.2 A word of caution

Confirmed LBVs AG Car and R127 are Ofpe/WN9 stars when in their hot state. Thus, in principle, any Ofpe/WN9 star could become an LBV as far as we know. Of(pe)/WNh stars will show He II λ4686 and strong [N II] emission lines.

While all Ofpe/WN9 stars could be cLBVs, there are other stars that can be cLBVs. At the lower luminosity end, the S Doradus instability strip is at lower temperatures, so quiescent/hot LBVs (at visual minimum brightness) are not so hot, and they do not have He II emission. Some do not even have He I emission, and some have pretty weak Balmer emission. In other words, having some criteria to select LBVs (like an Hα equivalent width stronger than some value, or the presence of an Ofpe/WN9 spectrum) will not produce a complete sample. There are some stars that might be dormant LBVs that will escape our criteria, especially at the lower luminosity end, i.e., at $\log(L/L_{\odot})$=5.3 to 5.8.

5.3 Candidate Wolf-Rayet stars

Classic W-R stars are the evolved descendants of massive stars with $\geq 25\,M_{\odot}$ which have completely lost their outer hydrogen, are fusing helium in the core, and are characterized by dense, He-enriched winds, which show prominent broad emission lines of ionised helium and highly ionised nitrogen or carbon. The last seven rows of Figure 10 (rows with IDs in white) show the MUSE cLBVs with broad He II λ4686 emission detections. Note that candidates #4 and #18 are too close to establish which of them is producing the He II and N III emission bumps which are observed in their spectra. Candidates #5, #10, #20, and #30 are also very close to each other. Their spectra, are characterized by an unusually-broad He II emission profile. This unusual profile could be explained by mutual contamination of these sources, if several of them emit in He II. Candidates #29 and #32 also show He II and N III emission bumps. For each MUSE cLBV, column 4 of Table 4 says which cLBVs show broad He II λ4686 emission. In column 4 of Table 4 we identify the cLBVs with the unusually broad He II profile with an asterisk.

Della Bruna et al. independently identified candidate W-R stars in NGC 7793W based on a MUSE He II surface brightness map. We use the coordinates provided by the latter authors to check if we have candidate W-R stars in common. The candidate W-R stars which we have in common are identified with a dagger in column 4 of Table 4. In Figure 10, the upper-left corner gives the ID of the candidate W-R star given by Della Bruna et al.. Because the spatial resolution of the *HST* images is greater than that of the MUSE data, we find cases where several of our MUSE cLBVs are in the region where Della Bruna et al. found a candidate W-R star based on the MUSE data.

We noticed that Della Bruna et al. found five candidate W-R stars which are not part of our MUSE cLBV sample. Figure 12 shows postage stamps of the latter candidates. The postage stamps are centered on the MUSE coordinates provided by Della Bruna et al. (orange markers), which correspond to the MUSE He II centroid. The slight offset between the orange markers and point *HST* sources in the figure can be explained by the pixel scale of the MUSE data, which is 0.2″. This corresponds to five *HST* pixels. Thus, the offset is within a distance of five random *HST* pixels from the *HST* centering. In four cases, we did not select the source as a photometric cLBV because the source failed to pass our roundness or sharpness criteria. However, in the case of

WR5, we did not select it because after subtracting the continuum from the Hα filter, the source did not pass our Hα luminosity criterion.

6   DISCUSSION

6.1   Isolation of cLBVs

Smith (2019) argued that LBVs are isolated from locations of star formation. As explained in the introduction, this would favor a binary formation scenario for LBVs. Table 3 shows that our five strongest cLBVs are at least 7 pc away in projection on the sky from young star clusters; and that three of them are outside of large H II region complexes. Table 3 also shows that several candidate O-type stars are located within 7 pc of our top five cLBVs. Thus, at this point, we cannot conclude if our promising cLBVs are isolated from bona-fide O-type stars or not. Follow-up of these not yet confirmed LBVs could help determine the properties and fraction of LBVs that follow the binary channel.

6.2   cLBVs in other LEGUS galaxies

Two other LEGUS galaxies are sufficiently close to search for photometric cLBVs using the method presented in this work, NGC 1313 (4.39 Mpc, Calzetti et al. 2015) and NGC 4395 (4.3 Mpc, Calzetti et al. 2015). For NGC 1313 (southern hemisphere), we already secured optical spectroscopy with Gemini Multi-Object Spectrograph South. We had two masks designed for the NGC1313 field. The first mask got a total of 26 sources in the slits and the second one 19 sources. Both of them were observed in good conditions on Dec 1 and 12, 2018 (first mask) and Jan 1 and 4, 2019 (second one). We used a slit width of 0.75âĂİ. The analysis is underway. For NGC 4395 (northern hemisphere), we have failed so far to obtain observations with the OSIRIS MOS on Gran Telescopio Canarias. Since the 0.8" slit is larger than the *HST* spatial resolution (0.1 arcsec), contamination from nearby sources in the slit would need to be considered, as we did in the present work.

7   SUMMARY AND CONCLUSIONS

Bona-fide LBVs are extraordinarily rare, with only ~44 known in 8 galaxies covering a wide range of metallicities and morphologies, including 19 in the Milky Way. Candidate LBVs are also rare, with about 124 known in 12 galaxies. The confirmed LBVs are incompletely characterized, because they require multi-epoch high-spatial resolution imaging and spectroscopy, spanning several decades. This is why searching for cLBVs in new galaxies with good quality data, such as the three nearest galaxies in LEGUS, is so important. Such observations are seminal in order to establish the maximum luminosity of LBVs and the duration of the LBV phase.

We combine WFC3 images of NGC 7793W in the F547M, F657N and F814W filters, with restrictions of roundness, sharpness and Hα luminosity, to produce a catalogue of potential cLBVs (photometric cLBVs). We focus on the subset of the latter sources which have MUSE spectroscopy, finding five strong cLBV candidates. Our five

strongest candidates would benefit from follow up observations in order to be confirmed as bona-fide LBVs. In addition, we find three strong candidate Wolf-Rayet stars. Additional Wolf-Rayet stars have been found in the galaxy by other authors but they do not pass our selection criteria for the photometric cLBVs. At this point, we are unable to favor the binary formation scenario for LBVs. We note that the most luminous photometric cLBVs in NGC 7793 were not observed with MUSE AO and are worth following-up spectroscopically, along with photometric cLBVs in other LEGUS galaxies.

REFERENCES

Adamo A., et al., 2017, ApJ, 841, 131
Asplund M., Grevesse N., Sauval A. J., Scott P., 2009, ARA&A, 47, 481
Bacon R., et al., 2010, in Ground-based and Airborne Instrumentation for Astronomy III. p. 773508, doi:10.1117/12.856027
Baldwin J. A., Phillips M. M., Terlevich R., 1981, PASP, 93, 5
Belczynski K., Holz D. E., Bulik T., O'Shaughnessy R., 2016, Nature, 534, 512
Bell E. F., de Jong R. S., 2001, ApJ, 550, 212
Berg D. A., Skillman E. D., Garnett D. R., Croxall K. V., Marble A. R., Smith J. D., Gordon K., Kennicutt Jr. R. C., 2013, ApJ, 775, 128
Bessell M. S., 1990, PASP, 102, 1181
Bonanos A. Z., et al., 2006, ApJ, 652, 313
Bothwell M. S., Kennicutt R. C., Lee J. C., 2009, MNRAS, 400, 154
Bresolin F., 2007, ApJ, 656, 186
Bresolin F., 2011, ApJ, 730, 129
Bressan A., Marigo P., Girardi L., Salasnich B., Dal Cero C., Rubele S., Nanni A., 2012, MNRAS, 427, 127
Calzetti D., et al., 2015, AJ, 149, 51
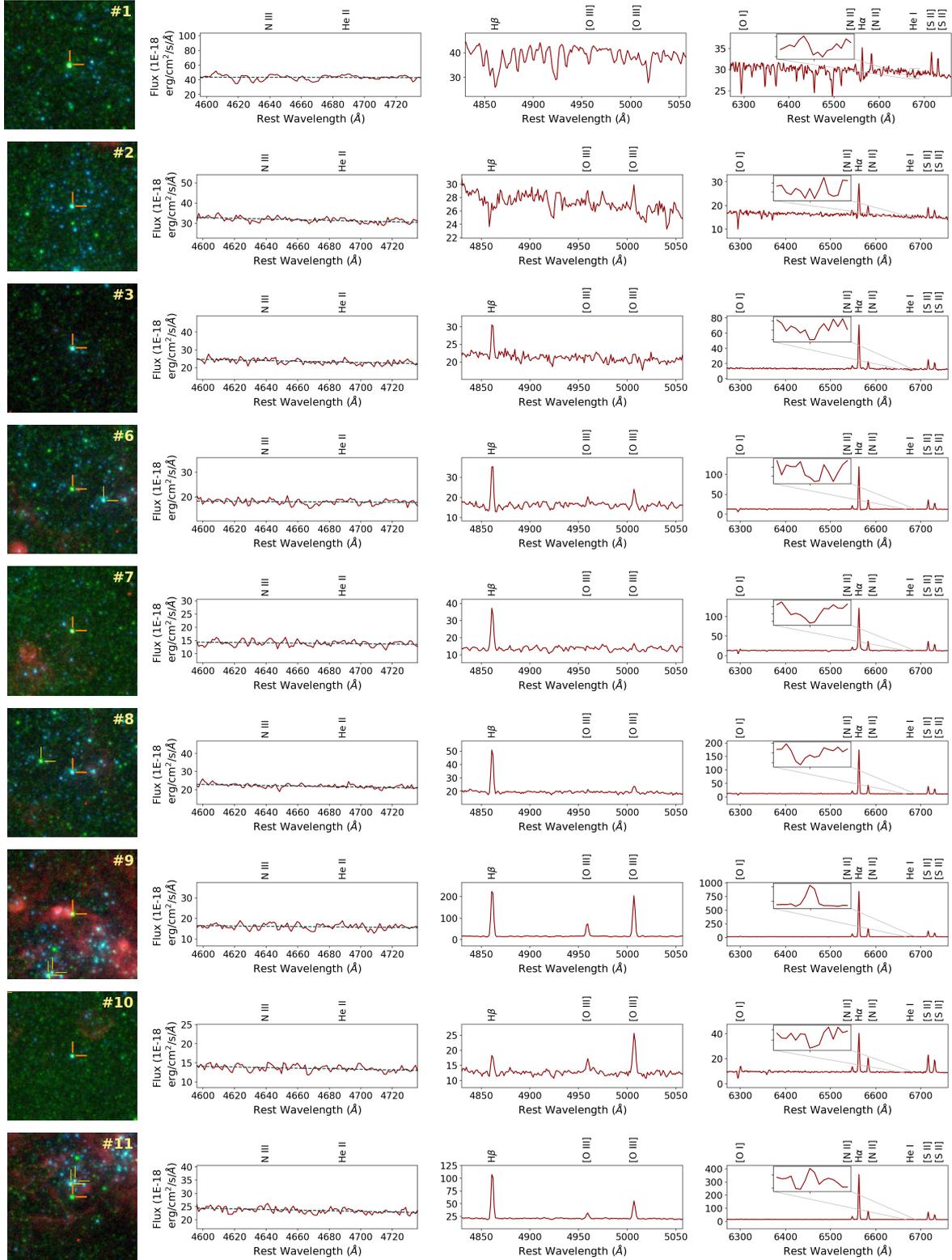Castro N., et al., 2008, A&A, 485, 41

Figure 7. Postage stamps and portions of MUSE spectra of nine MUSE cLBVs whose ID is given in the upper-right corner of the postage stamp. The postage stamps are RGB composite images where blue corresponds to F275W + F336W, green to F438W + F814W, and red to F657N. At the adopted distance of 3.44 Mpc, 0.6" represent ~10 pc. The markers are 10 pc in length and the images 120 pc on the side. Yellow tick marks correspond to other MUSE cLBVs in the field. The spectra are extracted from circular regions of 0.8" in diameter centred on the cLBVs. We present spectra which are corrected for extinction in the Milky Way and redshift. In the panel showing He II, the dashed curve corresponds to a fit to the He II continuum. The inset on the right-most panel shows an enlargement of the He I λ6678 line. The tick mark on the x-axis corresponds to 6678 Å.
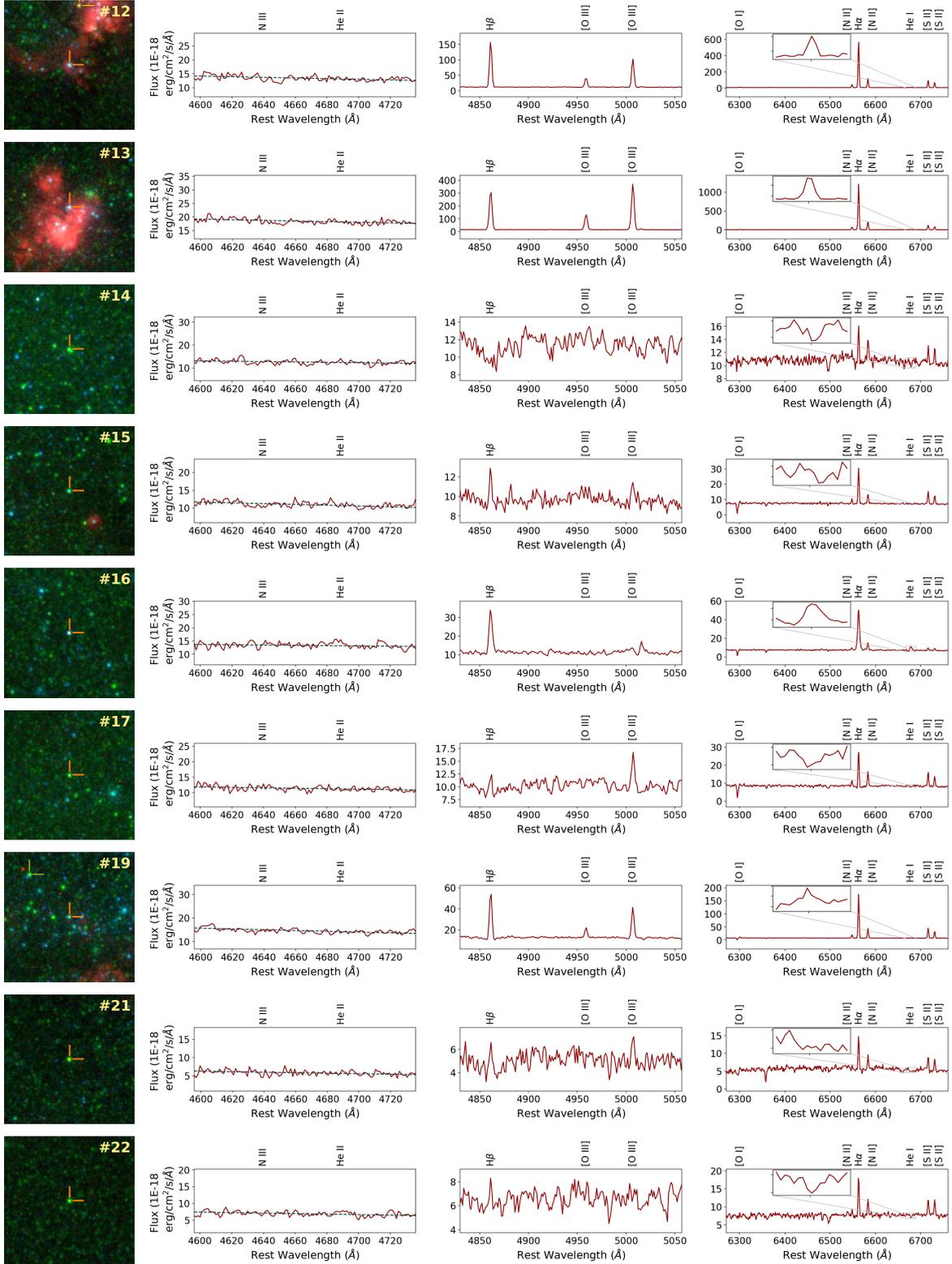
Figure 8. Same as Figure 7 but for a different set of MUSE cLBVs.

Clark J. S., Larionov V. M., Arkharov A., 2005, A&A, 435, 239

Clark J. S., Castro N., Garcia M., Herrero A., Najarro F., Negueruela I., Ritchie B. W., Smith K. T., 2012, A&A, 541, A146

Conti P. S., 1975, Memoires of the Societe Royale des Sciences de Liege, 9, 193

Davidson K., Humphreys R. M., Weis K., 2016, arXiv e-prints, p. arXiv:1608.02007

Dopita M. A., Seitenzahl I. R., Sutherland R. S., Nicholls D. C., Vogt F. P. A., Ghavamian P., Ruiter A. J., 2019, AJ, 157, 50
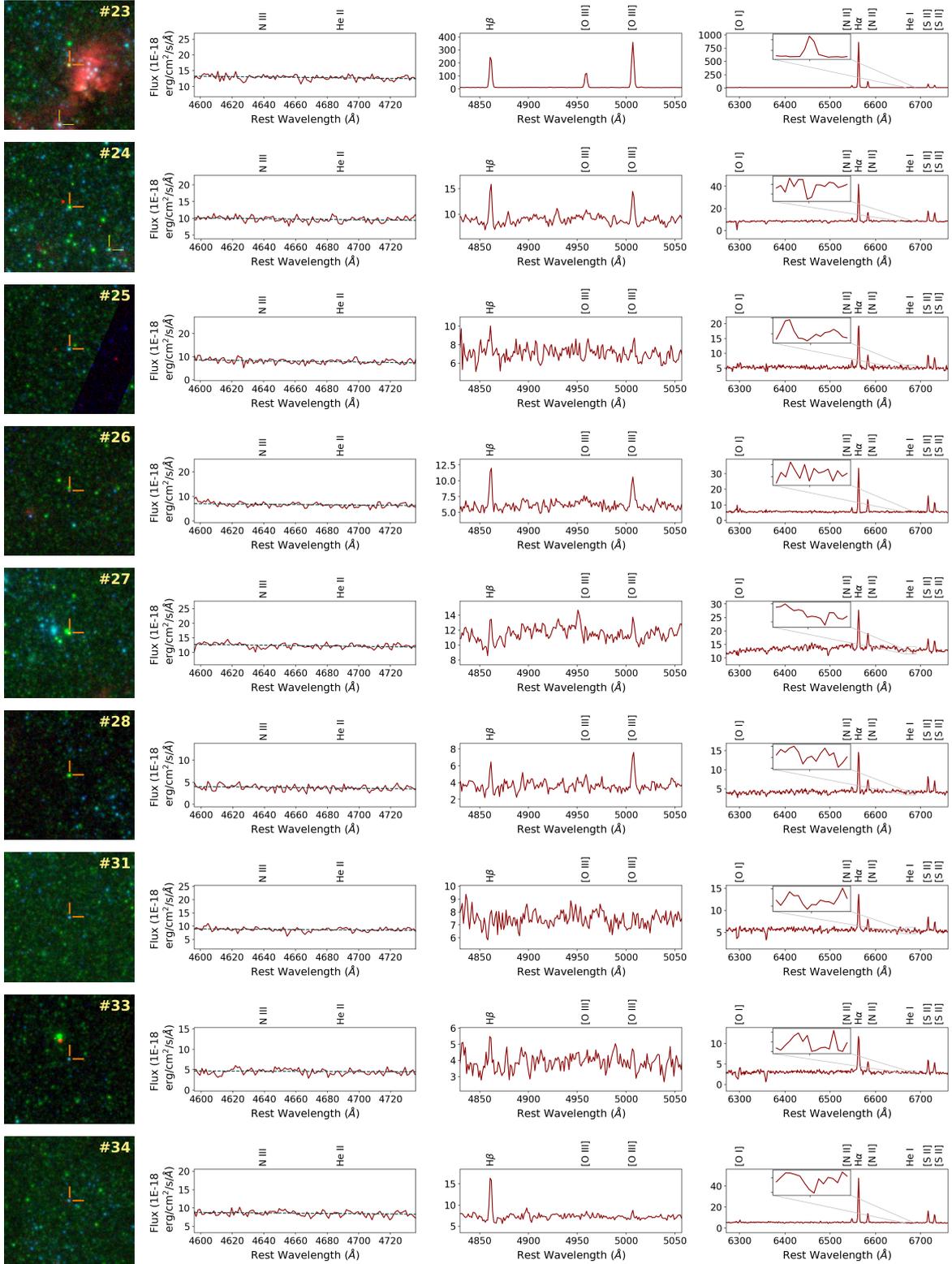
Figure 9. Same as Figures 7 and 8 but for a different set of MUSE cLBVs.

Drissen L., Crowther P. A., Smith L. J., Robert C., Roy J.-R., Hillier D. J., 2001, ApJ, 546, 484

Freedman W. L., et al., 2001, ApJ, 553, 47

Garnett D. R., Shields G. A., 1987, ApJ, 317, 82

Garnett D. R., Skillman E. D., Dufour R. J., Peimbert M., Torres-

Peimbert S., Terlevich R., Terlevich E., Shields G. A., 1995, ApJ, 443, 64

Grammer S. H., Humphreys R. M., Gerke J., 2015, AJ, 149, 152

Grasha K., et al., 2017, ApJ, 842, 25

Grasha K., et al., 2018, MNRAS, 481, 1016

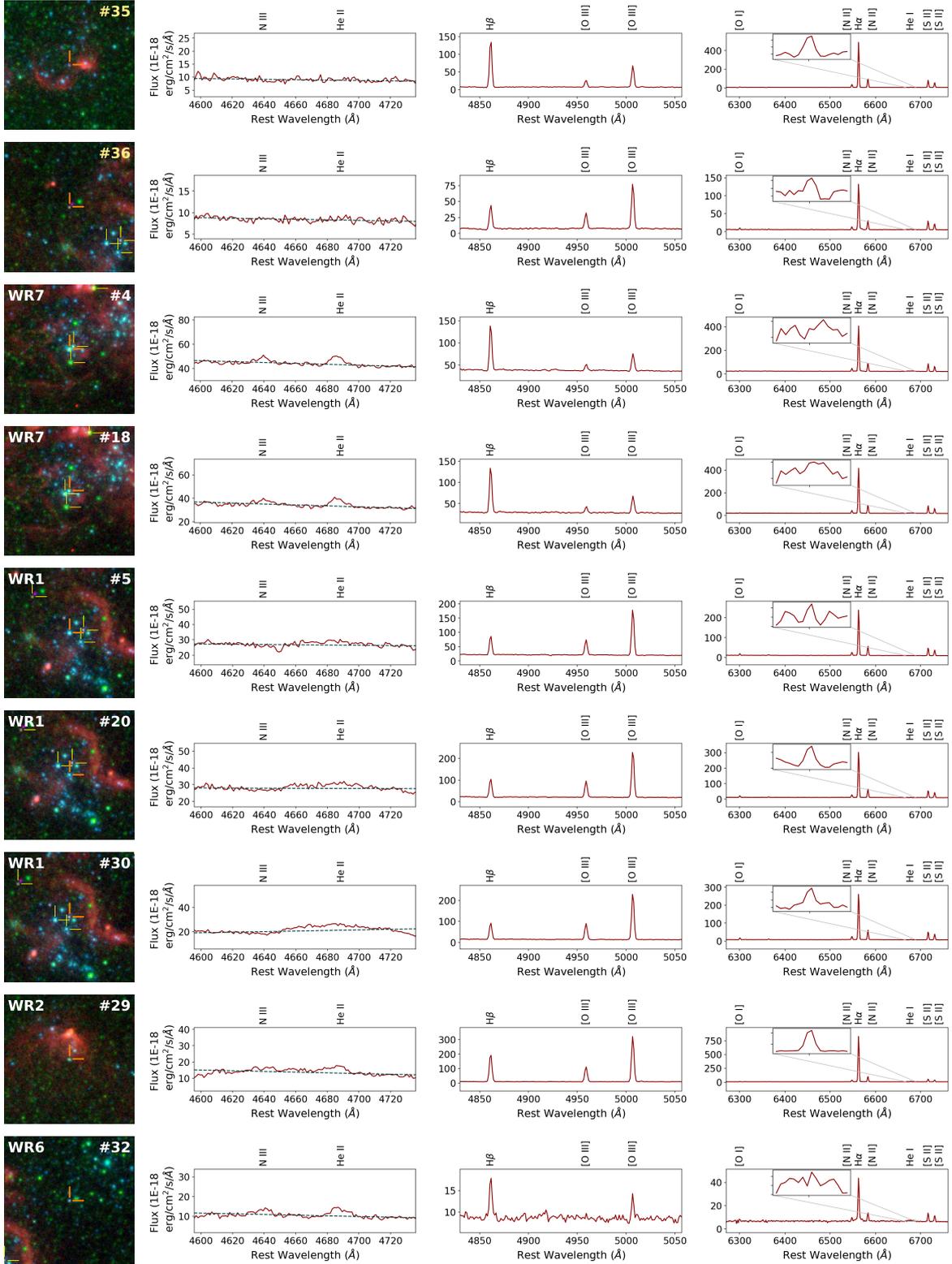**Figure 10.** Same as Figures 7, 8, and 9, except for a different set of MUSE cLBVs. The last seven rows show the MUSE cLBVs with detections of the N III *λ*4640 and/or He II *λ*4686 bumps.

Table 4. Spectroscopic properties of MUSE cLBVs.

ID	FWHM(Hα)[a]	He I[b]	He II[b]	[O I][b]	$\frac{F([OIII]5007)}{F(H\beta)}$ [c]	$\frac{F([NII]6584)}{F(H\alpha)}$ [c]	$\frac{F([SII]6716)}{F([SII]6731)}$ [c]
(1)	(2)	(3)	(4)	(5)	(6)	(7)	(8)
1	120 ± 15	0	0	0	Hβ in absorption, No [O III] emission	0.56	1.22
2	132 ± 5	0	0	0	Hβ in absorption	0.29	1.11
3	130 ± 1	0	0	0	No [O III] emission	0.15	1.40
4	126 ± 1	1	1	1	0.40	0.17	1.43
5	126 ± 1	1	1*	1	2.46	0.19	1.39
6	122 ± 1	0	0	0	0.37	0.24	1.38
7	133 ± 1	0	0	1	No [O III] emission	0.19	1.41
8	122 ± 1	0	0	1	0.19	0.20	1.41
9	128 ± 1	1	0	1	0.81	0.19	1.43
10	135 ± 1	0	0	1	2.81	0.38	1.36
11	126 ± 1	1	0	1	0.41	0.20	1.49
12	120 ± 1	1	0	1	0.62	0.19	1.44
13	129 ± 1	1	0	1	1.17	0.17	1.43
14	133 ± 12	0	0	0	Hβ in absorption, No [O III] emission	0.86	0.96
15	129 ± 2	0	0	0	0.94	0.26	1.40
16	138 ± 9	1	1*	0	0.58	0.12	1.08
17	128 ± 2	0	0	0	1.96	0.37	1.32
18	124 ± 1	1	1†	1	0.39	0.18	1.45
19	125 ± 1	1	0	1	0.69	0.23	1.46
20	126 ± 1	1	1	1	2.57	0.17	1.39
21	119 ± 7	0	0	0	0.59	0.36	1.31
22	119 ± 5	0	1*†	0	No [O III] emission	0.38	1.05
23	123 ± 1	1	0	1	1.43	0.14	1.45
24	128 ± 2	0	0	0	0.94	0.25	1.20
25	141 ± 4	0	0	1	No [O III] emission	0.26	1.21
26	123 ± 2	0	0	1	0.86	0.29	1.56
27	155 ± 7	0	0	0	0.34	0.33	0.98
28	135 ± 4	0	0	0	2.33	0.34	1.45
29	124 ± 1	1	1†	1	1.59	0.11	1.47
30	128 ± 1	1	1*†	1	2.80	0.19	1.40
31	128 ± 12	0	0	0	Hβ in absorption, No [O III] emission	0.29	1.36
32	127 ± 2	0	1	1	0.46	0.19	1.32
33	155 ± 8	0	0	1	No [O III] emission	0.27	1.27
34	126 ± 1	0	0	1	0.17	0.21	1.37
35	121 ± 1	1	0	1	0.45	0.20	1.46
36	131 ± 1	1	0	1	1.90	0.19	1.42
min	119				0.17	0.11	0.96
max	155				2.81	0.86	1.56
mean	129				1.12	0.25	1.34
median	127				0.81	0.20	1.40
σ					0.85	0.13	0.15

Notes

[a] Full width at half maximum of Hα line in km s⁻¹ measured from MUSE spectrum after correction for extinction in the Milky Way. When an underlying stellar absorption component is present, we fit that component. When a broader emission component is present, we also fit that component. We give the FWHM corresponding to the narrow emission component to Hα. Weaker components to the line may include underlying stellar absorption and/or a broader emission component.

[b] Presence of He I λ6678, broad He II λ4686, and [O I] λ6300 emission lines in the MUSE cLBV spectra. 1=the line was detected. 0=the line was undetected. Asterisk in column 4=extremely broad He II λ4686 detection. † in column 4=cLBV identified as candidate W-R candidate in Della Bruna et al. (subm.).

[c] Emission line flux ratio or comment about the ratio.

Groenewegen M. A. T., 2013, A&A, 550, A70

Hannon S., et al., 2019, arXiv e-prints, p. arXiv:1910.02983

Herrero A., Garcia M., Uytterhoeven K., Najarro F., Lennon D. J., Vink J. S., Castro N., 2010, A&A, 513, A70

Hollyhead K., Bastian N., Adamo A., Silva-Villa E., Dale J., Ryon J. E., Gazak Z., 2015, MNRAS, 449, 1106

Humphreys R. M., Davidson K., 1994, PASP, 106, 1025

Humphreys R. M., Weis K., Davidson K., Bomans D. J., Burggraf B., 2014, ApJ, 790, 48

Humphreys R. M., Gordon M. S., Martin J. C., Weis K., Hahn D., 2017a, ApJ, 836, 64

Humphreys R. M., Davidson K., Van Dyk S. D., Gordon M. S., 2017b, ApJ, 848, 86

Humphreys R. M., Stangl S., Gordon M. S., Davidson K., Grammer S. H., 2019, AJ, 157, 22

Izotov Y. I., Guseva N. G., Fricke K. J., Henkel C., 2011, A&A, 533, A25

Johnson H. L., Morgan W. W., 1953, ApJ, 117, 313

Kahre L., et al., 2018, ApJ, 855, 133

King N. L., Walterbos R. A. M., Braun R., 1998, ApJ, 507, 210

Koenigsberger G., Georgiev L., Hillier D. J., Morrell N., Barbá R., Gamen R., 2010, AJ, 139, 2600

Krumholz M. R., et al., 2015, ApJ, 812, 147

Lee J. C., et al., 2009, ApJ, 706, 599

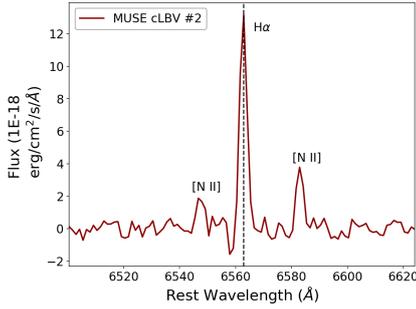**Figure 11.** Hα line with P-Cygni like profile of candidate #2.

Magrini L., Gonçalves D. R., 2009, MNRAS, 398, 280

Magrini L., Gonçalves D. R., Vajgel B., 2017, MNRAS, 464, 739

Maíz Apellániz J., 2006, AJ, 131, 1184

Massey P., McNeill R. T., Olsen K. A. G., Hodge P. W., Blaha C., Jacoby G. H., Smith R. C., Strong S. B., 2007, AJ, 134, 2474

Miroshnichenko A. S., et al., 2014, Advances in Astronomy, 2014, E7

Pellerin A., Macri L. M., 2011, ApJS, 193, 26

Pietrzyński G., et al., 2010, AJ, 140, 1475

Pilyugin L. S., Grebel E. K., Kniazev A. Y., 2014, AJ, 147, 131

Polles F. L., et al., 2019, A&A, 622, A119

Pustilnik S. A., Makarova L. N., Perepelitsyna Y. A., Moiseev A. V., Makarov D. I., 2017, MNRAS, 465, 4985

Rich J. A., Persson S. E., Freedman W. L., Madore B. F., Monson A. J., Scowcroft V., Seibert M., 2014, ApJ, 794, 107

Richardson N. D., Mehner A., 2018, Research Notes of the American Astronomical Society, 2, 121

STSCI Development Team 2012, DrizzlePac: HST image software, Astrophysics Source Code Library (ascl:1212.011)

Sabbi E., et al., 2018, ApJS, 235, 23

Sacchi E., et al., 2019, ApJ, 878, 1

Schlafly E. F., Finkbeiner D. P., 2011, ApJ, 737, 103

Smith N., 2017, Philosophical Transactions of the Royal Society of London Series A, 375, 20160268

Smith N., 2019, MNRAS, 489, 4378

Smith N., Tombleson R., 2015, MNRAS, 447, 598

Smith L. J., Nota A., Pasquali A., Leitherer C., Clampin M., Crowther P. A., 1998, ApJ, 503, 278

Stanghellini L., Magrini L., Casasola V., Villaver E., 2014, A&A, 567, A88

Tang J., Bressan A., Rosenfield P., Slemer A., Marigo P., Girardi L., Bianchi L., 2014, MNRAS, 445, 4287

Taylor M., 2011, TOPCAT: Tool for OPerations on Catalogues And Tables, Astrophysics Source Code Library (ascl:1101.010)

Tully R. B., et al., 2013, AJ, 146, 86

Van Dyk S. D., Matheson T., 2012, in Davidson K., Humphreys R. M., eds, Astrophysics and Space Science Library Vol. 384, Eta Carinae and the Supernova Impostors. p. 249, doi:10.1007/978-1-4614-2275-4_11

Vink J. S., 2012, in Davidson K., Humphreys R. M., eds, Astrophysics and Space Science Library Vol. 384, Eta Carinae and the Supernova Impostors. p. 221 (arXiv:0905.3338), doi:10.1007/978-1-4614-2275-4_10

Wagner-Kaiser R., Sarajedini A., Dalcanton J. J., Williams B. F., Dolphin A., 2015, MNRAS, 451, 724

Walborn N. R., Gamen R. C., Morrell N. I., Barbá R. H., Fernández Lajús E., Angeloni R., 2017, AJ, 154, 15

Weilbacher P. M., Streicher O., Urrutia T., Pécontal-Rousset A., Jarno A., Bacon R., 2014, in Manset N., Forshay P., eds, Astronomical Society of the Pacific Conference Series Vol. 485,

Astronomical Data Analysis Software and Systems XXIII. p. 451 (arXiv:1507.00034)

Whitmore B. C., et al., 2011, ApJ, 729, 78

Wolf B., Stahl O., 1982, A&A, 112, 111

Zurita A., Bresolin F., 2012, MNRAS, 427, 1463

van Genderen A. M., 2001, A&A, 366, 508

APPENDIX A: *HST* PHOTOMETRY OF MUSE CLBVS.

The apparent Vega magnitudes in the seven filters used in this work are presented in Table A1, uncorrected for foreground or intrinsic extinction.

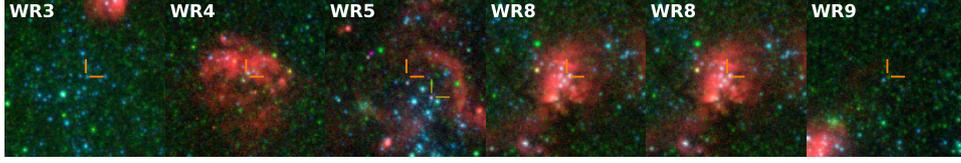This paper has been typeset from a TEX/LATEX file prepared by the author.

Figure 12. LEGUS/Hα-LEGUS postage stamps of the candidate W-R stars which we do not classify as photometric cLBVs and which were found by Della Bruna et al.. The images are centred on the MUSE He II centroid (orange tick marks, see text for explanation of the slight offset between the MUSE and *HST* coordinates. The spectra of these objects are presented in Della Bruna et al..

Table A1. Apparent Vega magnitudes of MUSE cLBVs based on *HST* PSF-photometry.

ID	F275W	F336W	F438W	F547M	F555W	F657N	F814W
1	22.291±0.027	20.668±0.012	19.857±0.004	19.233±0.004	19.388±0.003	18.751±0.007	18.744±0.003
2	19.686±0.007	19.304±0.006	20.004±0.004	19.974±0.006	19.888±0.003	19.631±0.010	19.738±0.004
3	19.015±0.005	18.984±0.005	20.140±0.004	20.089±0.006	20.047±0.004	19.731±0.011	19.816±0.005
4	19.073±0.005	19.066±0.005	20.245±0.005	20.116±0.007	20.138±0.004	19.727±0.011	19.875±0.005
5	18.396±0.004	18.851±0.005	20.375±0.005	20.577±0.008	20.512±0.004	20.350±0.015	20.598±0.006
6	23.652±0.073	22.267±0.031	21.407±0.011	20.608±0.008	20.705±0.005	20.092±0.013	19.873±0.004
7	22.315±0.027	21.843±0.020	21.752±0.010	20.796±0.009	20.720±0.005	19.806±0.011	19.707±0.004
8	19.325±0.008	19.476±0.008	20.904±0.009	20.898±0.010	20.762±0.005	20.585±0.018	20.667±0.007
9	24.511±0.112	22.632±0.032	21.599±0.009	20.719±0.009	20.811±0.005	19.912±0.013	19.697±0.004
10	20.831±0.012	20.350±0.010	21.008±0.008	20.819±0.009	20.840±0.005	20.354±0.015	20.469±0.006
11	24.015±0.076	22.503±0.029	21.731±0.010	21.073±0.013	20.989±0.005	20.332±0.019	19.971±0.005
12	19.233±0.006	19.591±0.006	21.031±0.007	21.118±0.011	21.170±0.006	20.811±0.020	21.117±0.008
13	19.330±0.006	19.626±0.007	21.081±0.007	21.149±0.011	21.174±0.006	20.844±0.022	21.162±0.009
14	24.814±0.125	22.784±0.036	21.989±0.011	21.177±0.011	21.286±0.006	20.490±0.016	20.260±0.006
15	21.967±0.022	21.210±0.014	21.469±0.008	21.353±0.012	21.382±0.007	20.857±0.019	20.846±0.007
16	19.551±0.006	19.937±0.008	21.473±0.008	21.599±0.014	21.421±0.007	20.683±0.017	21.372±0.010
17	0.000±0.000	22.948±0.037	22.230±0.013	21.507±0.013	21.488±0.007	20.849±0.019	20.691±0.007
18	20.296±0.010	20.374±0.010	21.565±0.009	21.496±0.013	21.623±0.008	20.978±0.022	21.090±0.009
19	22.092±0.024	21.585±0.018	21.780±0.010	21.607±0.023	21.641±0.008	21.216±0.029	21.351±0.010
20	19.526±0.007	20.012±0.008	21.501±0.009	22.005±0.016	21.730±0.008	21.582±0.029	21.849±0.013
21	0.000±0.000	0.000±0.000	24.273±0.040	21.811±0.015	0.000±0.000	20.376±0.014	19.918±0.004
22	0.000±0.000	0.000±0.000	23.455±0.024	21.678±0.014	21.826±0.008	20.710±0.017	20.351±0.006
23	22.914±0.044	22.404±0.030	22.198±0.013	21.880±0.015	21.839±0.009	20.743±0.019	21.327±0.011
24	22.938±0.039	23.222±0.046	23.364±0.024	21.858±0.026	21.898±0.009	20.736±0.021	20.222±0.005
25	20.599±0.011	20.809±0.012	22.037±0.011	22.191±0.018	22.112±0.010	21.776±0.032	22.075±0.014
26	0.000±0.000	23.162±0.073	23.069±0.025	22.338±0.019	0.000±0.000	21.717±0.030	24.071±0.052
27	0.000±0.000	0.000±0.000	24.354±0.045	21.821±0.016	22.405±0.013	20.371±0.015	19.972±0.007
28	0.000±0.000	25.763±0.257	24.446±0.043	22.451±0.020	22.586±0.012	21.152±0.022	20.602±0.006
29	22.174±0.026	21.942±0.023	22.891±0.019	22.609±0.024	22.613±0.013	21.847±0.036	21.994±0.014
30	20.906±0.014	21.098±0.014	22.723±0.017	22.926±0.028	22.805±0.014	21.912±0.036	22.710±0.021
31	21.141±0.015	21.475±0.020	22.933±0.020	23.093±0.030	22.987±0.016	22.447±0.048	22.899±0.024
32	21.314±0.015	21.570±0.017	22.957±0.018	23.146±0.032	23.055±0.016	22.147±0.040	22.812±0.022
33	21.629±0.018	21.910±0.021	23.456±0.024	23.754±0.043	23.250±0.018	22.767±0.061	23.124±0.026
34	21.616±0.018	21.934±0.021	23.398±0.024	23.533±0.038	23.478±0.021	22.647±0.054	23.219±0.029
35	21.475±0.017	21.997±0.022	23.521±0.026	23.741±0.044	23.669±0.024	22.806±0.062	23.805±0.043
36	23.451±0.051	23.102±0.042	23.924±0.033	23.441±0.037	24.262±0.033	22.194±0.041	22.892±0.023